Master Thesis

Low-Carbon, Low-Temperature Bainite

Yang, Hong-Seok (梁 洪 碩)

Department of Ferrous Technology

(Computational Metallurgy)

Graduate Institute of Ferrous Technology

Pohang University of Science and Technology

2008

저탄소 저온 베이나이트

Low-Carbon, Low-Temperature Bainite

Low-Carbon, Low-Temperature Bainite

By
Yang, Hong-Seok
Department of Ferrous Technology
(Computational Metallurgy)
Graduate Institute of Ferrous Technology
Pohang University of Science and Technology

A thesis submitted to the faculty of Pohang University of Science and Technology in partial fulfillments of the requirements for the degree of Master of Science in the Graduate Institute of Ferrous Technology (Computational Metallurgy)

Pohang, Korea
20 December, 2007

Approved by

Prof. Lee, Hae Geon	Prof. Bhadeshia, H. K. D. H.
Major Advisor	Co-Advisor

Low-Carbon, Low-Temperature Bainite

Yang, Hong-Seok

This dissertation is submitted for the degree of Master of Science at the Graduate Institute of Ferrous Technology of Pohang University of Science and Technology. The research reported herein was approved by the committee of Thesis Appraisal

20 December, 2007

Thesis Review Committee

Chairman: Lee, Hae Geon

Member: De Cooman, B. C.

Member: Liu, Weijie

Member: Kim, In Gee

Preface

This dissertation is submitted for the degree of Master of Engineering in Computational Metallurgy at Pohang University of Science and Technology. The research described herein was conducted under the supervision of Professor H. K. D. H. Bhadeshia, Adjunct Professor of Computational Metallurgy in the Graduate Institute of Ferrous Technology, Pohang University of Science and Technology and Professor of Physical Metallurgy, University of Cambridge, between March 2006 and December 2007.

This work is to the best of my knowledge original, except where acknowledgements and references are made to previous work. Neither this, nor any substantially similar dissertation has been or is being submitted for any other degree, diploma or other qualification at any other university.

Part of this work has been submitted to appear in the following publications:

Hong-Seok Yang and H. K. D. H. Bhadeshia: Uncertainties in dilatometric determination of martensite start temperature. *Materials Science and Technology,* Vol.23 (2007) pp. 556-560

Hong-Seok Yang and H. K. D. H. Bhadeshia: Designing low-carbon, low-temperature bainite. *Materials Science and Technology, In press*

Hong-Seok Yang

December 2007

Acknowledgements

I am extremely grateful to my supervisor, Professor H. K. D. H. Bhadeshia, for his constant guidance, support, great friendship and for his unique and charming way of teaching the simplicity and beauty of science. And thanks to Professor Weijie Liu, Professor In Gee Kim and Professor Rongshan Qin for their advise, support and friendship.

I am grateful to Professor Sung Mo Jung for the manufacture of the alloy and to Professor Bruno C. de Cooman for access to equipment. And also to Sung Jin Kim and the other Materials Design group members for helping to do experiments and for discussions.

I would like to express my sincere thanks to all the people in the Graduate Institute of Ferrous Technology (GIFT) in Pohang University of Science and Technology, especially those members in Computational Metallurgy Laboratory (CML), for all their help and for all the happiness we shared. The life with CML members was quite pleasant and enjoyable.

I would like to thank Professor Hae-Geon Lee for introducing GIFT and kind encouragement when I joined GIFT. I acknowledge GIFT and POSCO for their financial support.

I thank all my friends for their encouragement and friendship. Every GIFT friend, class mate during undergraduate course and other every friend is precious for me.

I would like to thank Dr Young-Jun Park, Joo-Hyun Ryu, Jun-Hak Pak and Sung-Hwa Seo for help and friendship during being my stay in Cambridge.

Finally, I would like to take this opportunity to express my gratitude to my family members for their love, unfailing encouragement and support. Especially I would like to say thanks to my wife, Hyo Sun Kim, for her support, devotion and understanding.

MIS Yang, Hong-Seok
20062859 Low-Carbon, Low-Temperature Bainite
Department of Ferrous Technology (Computational Metallurgy) 2007, 69p
Advisor: Lee, Hae Geon and Bhadeshia, H. K. D. H, Text in English

Abstract

The purpose of the present work was to examine the possibility of the low-carbon low-temperature bainite. Theory predicts that it is impossible to make low-carbon super-bainite using nickel alloying in 0.1C-2Mn (wt %) system. Three chemical compositions were considered with different concentrations of nickel.

During the work, uncertainties in dilatometric determination of martensite-start temperatures were recognised. They were systemically analysed and methods for the dilatometric determination of the martensite start temperature of steels was discussed, with emphasis on noise in the experimental data. The methods were tested on new set of data. Relying on the first detection of expansion due to transformation is fraught with difficulties. Instead, an offset method was proposed which should enable independent investigators to reach the same conclusions given identical data. The technique at the same time preserves the notion that the early stages of martensite formation correspond to the start temperature. The uncertainty in the start temperature deduced using this method was about ± 12 ℃, better than the reported values of noise in published data. The work underlines the need to state the sensitivity of the analysis technique when quoting transformation temperatures.

The possibility of producing bainite at low temperatures by suppressing transformation using substitutional solutes has been investigated, as an alternative to using large carbon concentrations to achieve the same purpose. It is found that although transformation temperatures can indeed be suppressed in this way, the difference between the bainite and martensite–start temperatures diminishes. This, combined with the relatively low carbon concentration of the steels studied, promotes the coarsening of the microstructure via a coalescence of fine bainite plates, which may have detrimental consequences on the properties although this remains to be demonstrated. The study also reveals the need for a better interpretation of the bainite–start temperature to cover circumstances where the transformation times are unusually long.

Contents

Preface……... i

Acknowledgements…….....……. ii

Abstract…….....……iii

Nomenclature……..……..… vi

Ⅰ. Introduction – Literature Review……...…….……...…….1

1.1 Aim of the Work……..1

1.2 Bainitic transformation…….1

1.2.1 Invariant-Plane Strain……..….4

1.2.2 Incomplete Reaction…….6

1.3 Super-Bainite……....8

1.4 Low-Carbon Super-Bainite…….....11

1.5 Summary……....18

Ⅱ. Experimental…….……20

2.1 Alloy Production……20

2.2 Dilatometry……...…….21

2.2.1 Quenching Experiments (Measuring M_S)……..…….....21

2.2.2 Isothermal Experiments…….....21

2.3 Transmission Electron microscopy…….…….....……21

2.4 Optical Microscopy……..……...22

2.5 X-ray Diffraction……22

2.6 Hardness Tests……...22

Ⅲ. Martensite Start Temperatures……...23

3.1 Uncertainties in Dilatometric Determination of M_S……...23

3.1.1 Detection of Expansion……..27

3.1.2 Offset Method……31

3.1.3 Source of Error……...34

3.1.4 Summary……35

3.2 Measured Martensite-Start Temperatures……..35

Ⅳ. Low-Carbon Low-Temperature Bainite……..37

4.1 Dilatometric Data……...37

4.2 Characterization of the Transformation…….41

4.2.1 Optical Microscopy……41

4.2.2 Hardness Tests……...52

4.2.3 X-ray Diffraction……53

4.2.4 Transmission Electron Microscopy……54

4.3 Bainite-Start Temperatures……59

4.4 Analysis of the Transformation Temperatures……...59

4.5 Summary……61

Ⅴ. Summary & Future Work……...….62

5.1 Summary……....62

5.2 Future Work……...63

Ⅵ. References……..64

Nomenclature

Ac_1	Temperature at which a sample starts to transform to austenite during heating
Ac_3	Temperature at which a sample becomes fully austenitic during heating
Ae_1	Temperature separating the $\alpha + \gamma$ and α phase fields for a specific alloy
Ae_3	Temperature separating the $\alpha + \gamma$ and γ phase fields for a specific alloy
A'_{e3}	As Ae_3, but para-equilibrium boundary
a	Plate length
a_{Fe}	Lattice parameter of pure iron in ferrite phase
a_{α}	Lattice parameter of ferrite
a_{γ}	Lattice parameter of austenite
B_S	Bainite-start temperature
C	Intercept of trend line to austenite linear contraction
C_i	Constants, with i=1, 2, 3, …
c	Plate thickness
m	Slope of trend line to austenite linear contraction

G_{N}	Universal nucleation function, which is specifying the free energy change needed in order to obtain a detectable rate of nucleation for Widmanstätten ferrite and bainite.
$G_N^{\alpha'}$	Function specifying the critical value of $\Delta G^{\gamma\rightarrow\alpha}$ at the M_{S}
G_S	Molar strain energy
G_{SB}	Stored energy of bainite
G_{SW}	Stored energy of Widmanstätten ferrite
ΔG_2	Free energy change per mole of ferrite for equilibrium or para-equilibrium transformation
ΔG_3	Free energy change for the formation of a mole of ferrite nuclei with carbon diffusion
ΔG_m	Maximum molar free energy change accompanying nucleation
$\Delta G^{\gamma\rightarrow\alpha}$	Free energy change for transformation without composition change
$\Delta G^{\gamma\rightarrow\gamma'+\alpha}$	Free energy change for equilibrium transformation
$\bar{L}$	Mean lineal intercept
M_{S}	Martensite-start temperature
s	Shear component of invariant-plane strain
t	Bainitic plate thickness
T	Temperature

T_0	Temperature at which austenite and ferrite of the same composition have the same free energy
$T_0^{'}$	As T_0, but accounting for the stored energy of ferrite
T_{h}	The temperature below which the nucleation of displacive transformation first becomes possible at a detectable rate
$\left\|\dot{T}\right\|$	Cooling rate
V	Volume fraction
V_m	Molar volume of austenite
w_{i}^{γ}	Weight fraction of species i in phase γ
W_{S}	Widmanstätten ferrite start temperature
$\bar{x}$	Average mole fraction of carbon in an alloy
x_i^{α}	Mole fraction of species i in phase α
x_m	Maximum carbon super-saturation permitted in ferrite, on thermodynamic grounds
$x_{T_0'}$	Carbon concentration given by the $T_0^{'}$ curve.
x^{γ}	Carbon concentration in austenite
$x^{\alpha\gamma}$	Mole fraction of carbon in ferrite which is in equilibrium or para-equilibrium with ferrite
$x^{\gamma\alpha}$	Mole fraction of carbon in austenite which is in equilibrium or para-equilibrium with ferrite

α	Ferrite
α_b	Bainitic ferrite
$\alpha_m^{'}$	Martensitic ferrite
γ	Austenite
γ'	Carbon-enriched austenite
δ	Dilatational component of invariant-plane strain
ε	Strain value which specify off-set corresponding to specific martensite volume fraction
ϵ_γ	Trend line to austenite linear contraction
μ	Shear modulus of austenite
ν	Poisson ratio
σ	Standard deviation
$\Delta\sigma$	Contribution to strength
AFM	Atomic force microscope
APT	Atom probe tomography
BCC	Body-centered cubic
BCT	Body-centered tetragonal
FCC	Face-centered cubic

HAZ	Heat-affected zone
HV	Vickers Hardness
TEM	Transmission electron microscope
TRIP	Transformation-Induced Plasticity
TTT	Time Temperature Transformation
XRD	X-ray diffraction

Ⅰ. Introduction – Literature Review

1.1 Aim of the Work

Bainitic steels can be stronger when the bainitic plates become thinner. And the plates become thinner as the transformation temperature decreases; the latter can be happened using high-carbon alloys. High-carbon, high strength steels with extremely fine bainite have recently been developed (Caballero *et al*., 2002, 2005; Garcia *et al*., 2003a, 2003b, 2003c). However, large carbon concentration is associated with very brittle martensite formation during welding. The aim of the work is to examine the possibility of low-carbon low-temperature bainite which can in principle be welded.

1.2 Bainitic Transformation

Bainite is a non-equilbrium decomposition product of austenite which evolves when cooling at rates such that diffusion-controlled transformations such as pearlite are not possible and yet, the cooling is sufficiently slow to avoid diffusionless transformation into athermal martensite. Bainitic microstructures are generally described as non-lamellar aggregates of carbides and plate-shaped ferrite. As shown in fig. 1.1, bainite can be classified according to its morphology as upper or lower bainite. Upper bainite consists of clusters of platelets of ferrite which share identical crystallographic orientation which are intimately connected to the parent austenite phase in which they grow. Elongated cementite particles decorate the boundaries of these plates; the amount and continuity of the cementite layer depends on the steel carbon concentration.

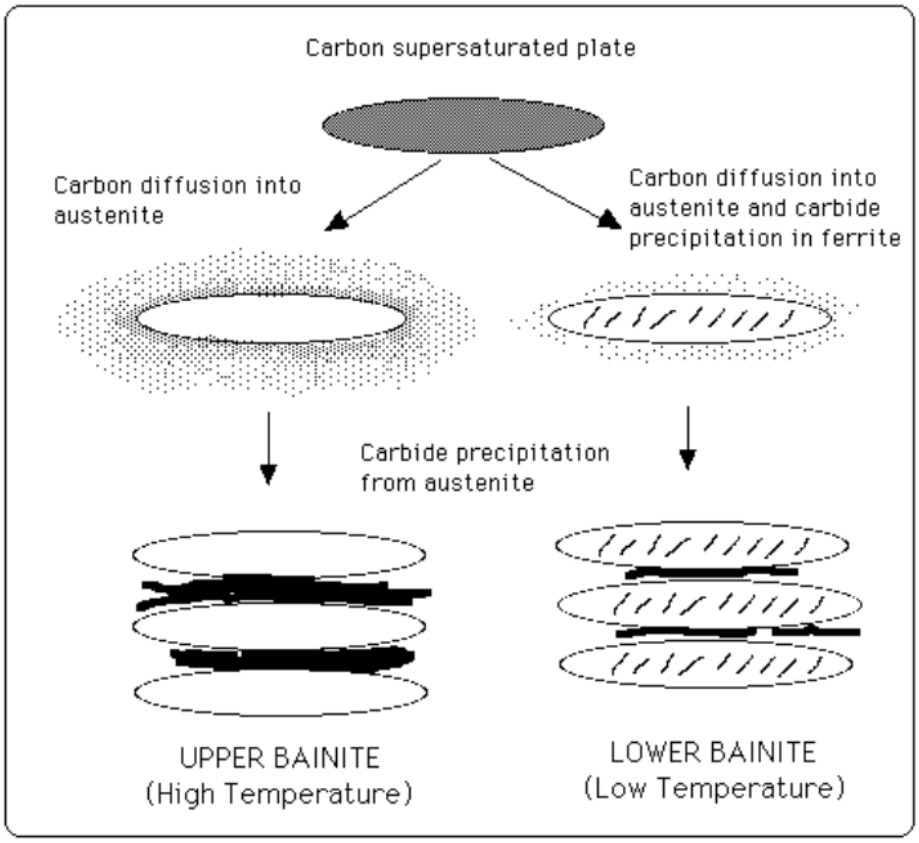

Fig. 1.1: Illustration of upper and lower bainite showing the main differences in carbon partitioning and precipitation behaviours (Takahashi and Bhadeshia, 1990).

Fully carbon-saturated bainitic ferrites are formed followed by carbon partitioning. The carbon escaping time is enough when the temperature is high, which results in upper bainite. As the transformation temperature is reduced, some of the carbon precipitates within the ferrite plates as cementite leading to lower bainite.

Very thin bainitic plates are called subunits because they grow in clusters known as sheaves. Within each sheaf, the subunits are parallel and of identical crystallographic orientation and habit plane. The microstructure can be seen using transmission electron microscopy (TEM) because the dimensions of bainite are too small to see using optical microscopy. The overall morphology of a sheaf is illustrated in fig. 1.2.

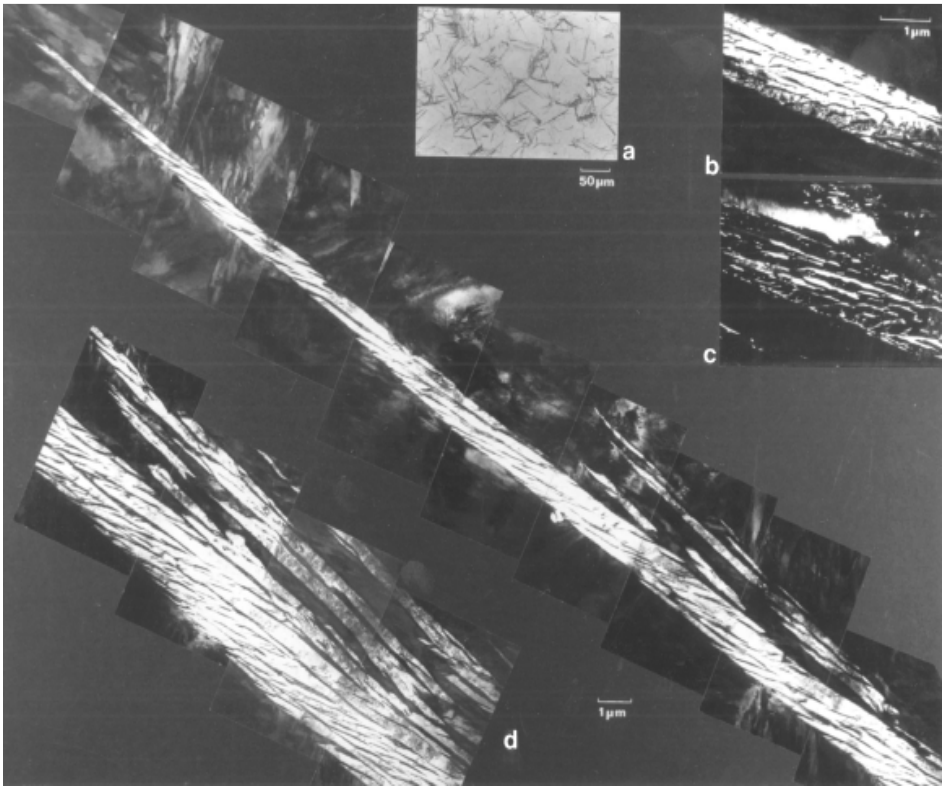

Fig. 1.2: Transmission electron micrograph of a sheaf of upper bainite in a partially transformed Fe-0.43C-2Si-3Mn wt % alloy: (a) light micrograph; (b, c) bright field and corresponding dark field image of retained austenite between the subunits; (d) montage showing the structure of the sheaf (Bhadeshia, 2001).

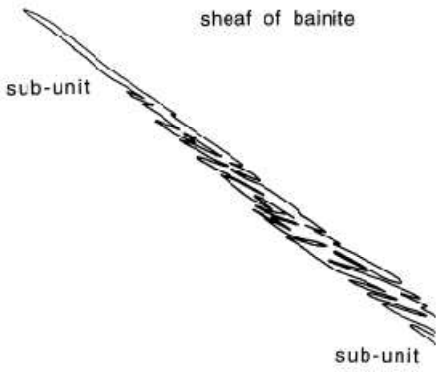

Fig. 1.2 (e): Corresponding outline of the subunits near the sheaf tip region (Bhadeshia, 2001).

1.2.1 Invariant-Plane Strain

There is no diffusion of iron atoms and substitutional elements when austenite transforms to Widmanstätten, bainitic and martensitic phases, so atoms move in disciplined manner in order to change the structure from face-centered cubic (fcc) to body-centered cubic (bcc) or body-centered tetragonal (bct). The Bain strain (Bain, 1924) is usually used to explain the deformation leading to the change in lattice. The Bain strain is a homogeneous pure deformation which can change the fcc crystal structure of austenite into the bcc or the bct structure of ferrite. This pure deformation can be combined with a rigid body rotation to give a net lattice deformation which leaves a single line unrotated and undistorted. In a situation where the transformation is constrained, such a low degree of fit between the parent and product lattices would lead to a great deal of strain as the product phase grows. However, by adding a further inhomogeneous lattice invariant deformation (shear or twinning), the combination of deformations appears macroscopically to be an invariant-plane strain (Swallow and Bhadeshia, 1996). An invariant-plane is one which is unrotated and undistorted, so that a greater degree of fit is achieved between the austenite and ferrite. This invariant-plane is also known as the habit plane, and the nature of the invariant-plane strain is illustrated in Table. 1.1. s and δ represent the shear and dilatational components of the strain.

Transformation	S	δ
Widmanstätten ferrite	0.36	0.03
Bainite	0.22	0.03
	0.26	
Martensite	0.24	0.03
Allotriomorphic α	0	0.03
Idiomorphic α	0	0.03

Table 1.1: Approximate values of the shear strain s and δ for a variety of transformation products in steels (Bhadeshia, 2001).

Dilatational strain is easy to understand, it comes from the difference in density between the bcc and fcc structure. There is no shear strain when austenite transforms in a reconstructive manner. Shear strain components of displacive transformations are huge, they exceed 20 %.

When an invariant-plane shape change has a large shear component, it implies at the very least coherency at the parent/product interface, which must be glissile (Swallow and Bhadeshia, 1996). These glissile interface movements during growth can be stopped when they meet forests of dislocations, which will be discussed later in detail. Another implication of an invariant-plane shape deformation is that the product phase must be in the form of a thin plate whose habit plane is the invariant plane. This is because the strain energy due to the invariant-plane shape deformation is then minimised (Christian, 1958). Widmanstätten ferrite plates tend to grow in a co-operative, mutually-accommodating manner, which can decrease the strain energy of plates. The calculated strain energy of Widmanstätten ferrite plate is about 50 J mol^{-1} and for bainitic plates is 400 J mol^{-1} (Bhadeshia, 1981a).

Both Widmanstätten ferrite and martensite can be obtained in the form of plates and its invariant plane shape change can be observed using an optical microscope. However, the microstructure of bainite consists of fine plates of ferrite, each of which is only about 0.2 μm in thickness, which is below the limit of resolution in light microscopy. Surface relief as a result of invariant-plane shape change during bainitic transformation has been observed using an atomic force microscope (AFM), which shows directly the surface relief of subunits of bainite (fig. 1.3). The plastic deformation shown in the fig. 1.3 will be discussed in later.

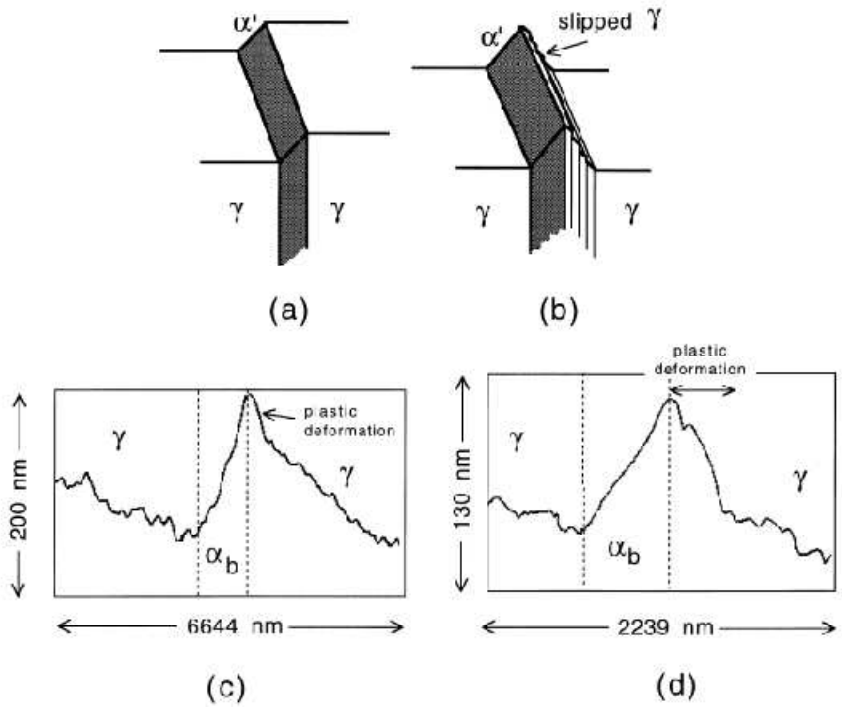

Fig. 1.3: (a) A perfect invariant plane strain surface relief effect. (b) One where plastic relaxation of the shape change occurs in the adjacent matrix. (c, d) An actual atomic force microscope scan across the surface relief due to a bainite sub-unit, the planes were flat before bainitic transformation (Swallow and Bhadeshia, 1996).

1.2.2 Incomplete Reaction

Fully bainitic steels are free from allotriomorphic ferrite and almost free from athermal martensite. The structure is thus composed of retained austenite, bainitic ferrite and carbides. Carbides, however, can be suppressed by alloying with elements such as silicon and aluminium. In order to understand the mechanism of bainite transformation, it is useful to consider a microstructure which does not contain carbides.

As shown in fig. 1.4, bainite growth by a diffusionless mechanism has to occur at a temperature just below T_0, when the free energy of bainitic ferrite falls below that of austenite of same composition (Zener, 1946). Ae_1 refers to the equilibrium (γ+α)/α phase boundary and Ae_3 refers to the equilbrium (γ+α)/γ phase boundary.

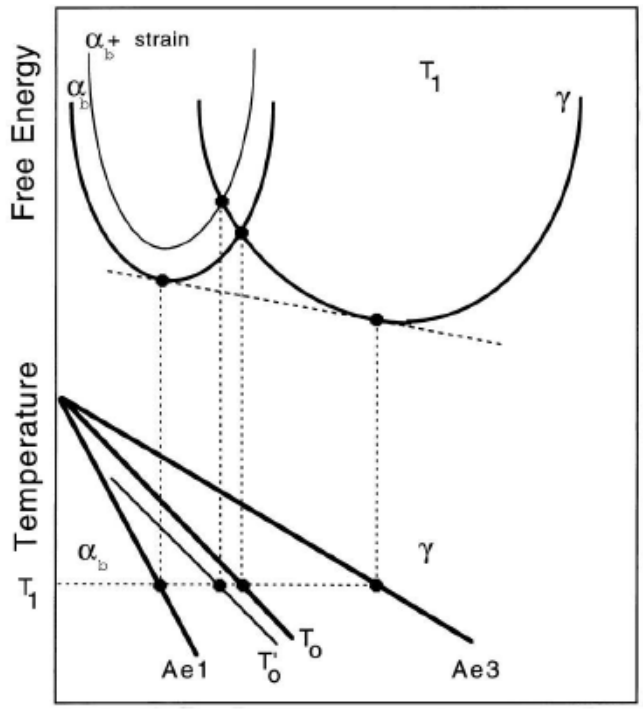

Fig. 1.4: Schematic illustration of the T_0 and $\boldsymbol{T_0'}$ curves (Bhadeshia, 2001). $\boldsymbol{T_0'}$ is same as T_0, but accounting for the stored energy of ferrite. T_1 is the temperature corresponding to the free energy curves. α_b refers to bainitic ferrite and γ austenite.

The stored energy in bainitic ferrite is accounted for by raising its free energy curve by an amount equal to the strain energy due to transformation, giving the T_0' curve. During isothermal transformation the excess carbon in the bainite partitions into the residual austenite, forcing the next plate to grow from carbon enriched austenite (Bhadeshia, 2001). The process finally ceases as the austenite carbon content reaches T_0' value, leading to the so called *incomplete reaction phenomenon* (Bhadeshia and Waugh, 1982). This is not true when carbides precipitate because they consume carbon and hence keep the concentration in the austenite below T_0 as transformation progresses.

The phenomenon makes it clear that carbon does not diffuse during bainitic growth. Carbon partitioning and carbide precipitation are just the next step of the transformation after the formation of supersaturated bainitic ferrite. If carbon atoms diffuse during transformation, the reaction must go on until the austenite composition reaches Ae_3 value, as in the case for Widmanstätten transformation which can be understood through the concept of para-equilibrium.

Atom probe tomography (APT) has been used to confirm directly the phenomenon (Bhadeshia and Waugh, 1982; Peet *et al*., 2004; Caballero *et al*., 2007; Pereloma *et al*. 2007). The atom probe technique makes it possible to see atoms and their positions with atomic scale spatial and chemical resolution. The dislocation densities of bainitic plates are quite large due to plastic relaxation (Bhadeshia and Edmonds, 1979). Actually, bainitic ferrite is somewhat in a saturated state even after carbon partitioning. This is because carbon atoms are trapped in the dislocations which are formed during plastic relaxation (Peet *et al*., 2004; Caballero *et al*., 2007).

1.3 Super Bainite

Bainitic sub-units grow up to a limited size, and are thin as mentioned earlier. The reason is that adjacent austenite phase cannot accommodate the shape deformation elastically. There is considerable plastic relaxation in the austenite adjacent to the bainite plates (fig. 1.3). The dislocation debris generated in this process resists the advance of the bainite/austenite interface, the resistance being greatest for strong austenite. The strength of austenite is the most important factor which determines the thickness of bainite (Singh and Bhadeshia, 1998). Because of that, the plates become thicker at high transformation temperatures since the yield strength of the austenite will then be lower.

There are also other factors such as driving force and the transformation temperature itself (Singh and Bhadeshia, 1998). A large driving force increases the nucleation rates. As a result, a larger driving force also leads to a finer microstructure. Though austenite strength is the most important factor that

determines the thickness of the bainite, austenite strength and free energy change during transformation are both influenced by temperature. A lower transformation temperature makes austenite strong and the driving force large. This leads to thinner plates of bainite. In order to get extremely fine bainite, it is necessary to transform at low temperatures.

There are two equations which account relationship between strength and grain size. One is the Hall-Petch equation and the other is due to Langford and Cohen. When the slip distance is less than about 1 μm, the Langford and Cohen relationship is more reasonable (Langford and Cohen, 1970). For a given thickness *t*, the mean lineal intercept, $\bar{L}$ is roughly two times the thickness and the strength contribution $\Delta\sigma$ due to the size of the plate is given by

$$\Delta\sigma = 115(\bar{L})^{-1}\,\text{MPa} \qquad (1.1)$$

where $\bar{L}$ is in micrometers according to Langford and Cohen relationship. It follows that $\Delta\sigma$ =311 MPa for plates of thickness 185 nm, whereas $\Delta\sigma$=1642 MPa for plates of thickness 35 nm, which means it's possible to get additional strength of more than 1 GPa without compromising toughness.

Extremely fine bainitic structures which consist of bainitic ferrite plates and carbon-enriched austenite without carbide precipitation have been developed (Caballero *et al*., 2002, 2005; Garcia *et al*., 2003a, 2003b, 2003c). This was achieved through bainitic transformation at temperatures as low as 200-125 ℃. The scale of the microstructure achieved is very fine indeed, amounting to tens of nanometers as shown in fig. 1.5. The microstructure exhibits an excellent combination of strength and ductility. The strength mainly comes from the fine scale of the structure rather than carbon even though the steels contain about 1 wt% of carbon.

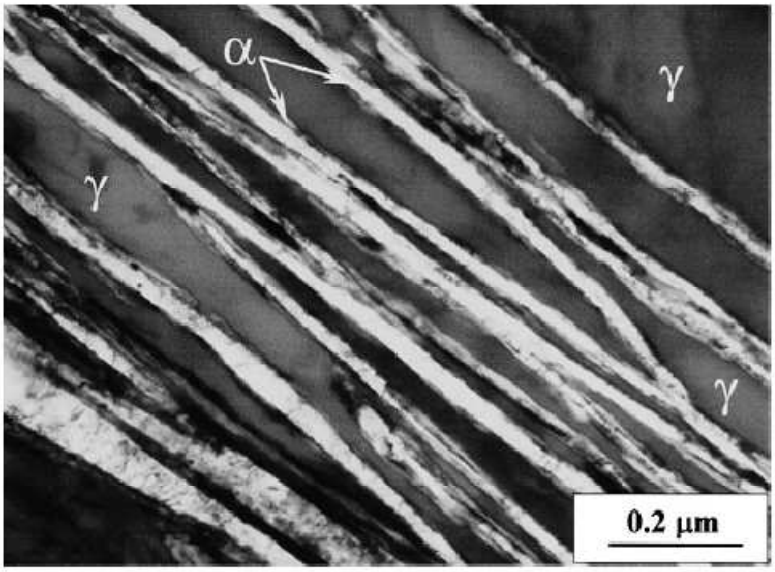

Fig. 1.5: Fe-0.98C-1.46Si-1.89Mn-0.26Mo-1.26Cr-0.09V wt %, Very fine structure: mixture of bainitic ferrite and retained austenite achieved through transformation at 200 ℃ for 5 days (Garcia *et al*., 2003c).

The applications, advantages, mechanical properties, characteristics and design strategies of these extremely fine carbide free bainitic structures are well described elsewhere (Bhadeshia, 1998; 2004; 2005a; 2005b; 2006a; 2007). Ultimate tensile strengths of 2500 MPa in tension have been routinely obtained, ductilities in the range 5-30 % and toughness in excess of 30-40 MPa $m^{1/2}$. The bainite is also the hardest ever achieved, 700 HV. The potential advantages of the mixed microstructure of bainitic ferrite and austenite can be listed as follows (Bhadeshia 1998):

(a) Cementite is responsible for initiating fracture in high–strength steels. Its absence is expected to make the microstructure more resistant to cleavage failure and void formation.

(b) The bainitic ferrite is almost free of carbon, which is known to embrittle ferritic microstructures.

(c) The microstructure derives its strength from the ultrafine grain size of the ferrite plates, which are less than 1 μm in thickness. It is the thickness of these plates which determines the mean free slip distance, so that the effective grain size is less than a micrometre. This cannot be achieved by any other commercially viable process. Grain refinement is the only method available for simultaneously improving the strength and toughness of steels.

(d) The ductile films of austenite which are intimately dispersed between the plates of ferrite have a crack blunting effect. They further add to toughness by increasing the work of fracture as the austenite is induced to transform to martensite under the influence of the stress field of a propagating crack. This is the TRIP, or transformation–induced plasticity effect.

(e) The diffusion of hydrogen in austenite is slower than in ferrite. The presence of austenite can therefore improve the stress corrosion resistance of the microstructure.

(f) Steels with the bainitic ferrite and austenite microstructure can be obtained without the use of any expensive alloying additions. All that is required is that the silicon concentration should be large enough to suppress cementite.

The most useful advantage of the steel is that the simple process route avoids rapid cooling so that residual stresses are avoided, even in large pieces. There are many adjectives that have been given to the bainitic microstructure described above: cold bainite, hard bainite, strong bainite and super bainite (Bhadeshia, 2004).

1.4 Low-Carbon Super-Bainite

Super-bainite is based on high-carbon steel, about 1 wt %. Such steels should be difficult to weld because of the possibility of untempered, brittle martensite in the coarse-grained heat affected zones (HAZ) of the joints. Such martensite fractures easily, leading to a gross deterioration in the structural integrity of the joint. For this reason, the vast majority of weldable steels have low-carbon concentrations. It

would be desirable therefore to make the super-bainite with a much reduced carbon concentration (Bhadeshia, 2006a). One criterion which should be satisfied in order to get super-bainite is that martensite-start temperature (M_S) should be low and bainite-start temperature (B_S) should be higher than M_S.

A theory which predicts the possibility of low-carbon super-bainite is available. The theory only relies on thermodynamics to predict the M_S and B_S. We can consider several kinds driving force when austenite transforms (fig. 1.7). $\Delta G^{\gamma\rightarrow\gamma'+\alpha}$ is the free energy change when austenite of composition $\bar{x}$ decomposes into the equilibrium mixture of ferrite and carbon-enriched austenite (γ'), fig. 1.7a. And the free energy change per mole of ferrite is ΔG_2

$$\Delta G_2 = \Delta G^{\gamma\rightarrow\gamma'+\alpha} \times \frac{x^{\gamma\alpha} - x^{\alpha\gamma}}{x^{\gamma\alpha} - \bar{x}} \tag{1.2}$$

where $x^{\alpha\gamma}$ and $x^{\gamma\alpha}$ are the equilibrium compositions of ferrite and austenite respectively. The calculation of the free energy change associated with nucleation must take account into that only a minute quantity of ferrite is formed. Consider the change ΔG_2 as austenite decomposes to a mixture of ferrite and enriched austenite of composition $x^{\gamma} = x^{\gamma\alpha}$. As the fraction of ferrite is reduced, x^{γ} and $\bar{x}$ move towards each other causing the line AB to tilt upwards. In the limit that $x^{\gamma} = \bar{x}$, AB becomes tangential to the curve at $\bar{x}$. The free energy change for the formation of a mole of ferrite nuclei of composition x^{α} is then given by ΔG_3, fig. 1.7b.

The greatest reduction in free energy during nucleation is obtained if the composition of the ferrite nucleus is set to a value x_m, given by a tangent to the ferrite free energy curve which is parallel to the tangent to the austenite free energy curve at $\bar{x}$, as shown in fig. 1.7b. This maximum possible free energy change for nucleation is designated ΔG_m.

There is simplification when the transformation occurs without composition change. The change $\Delta G^{\gamma\rightarrow\alpha}$ is the vertical distance between the austenite and ferrite energy curves at the composition of interest (fig. 1.7c).

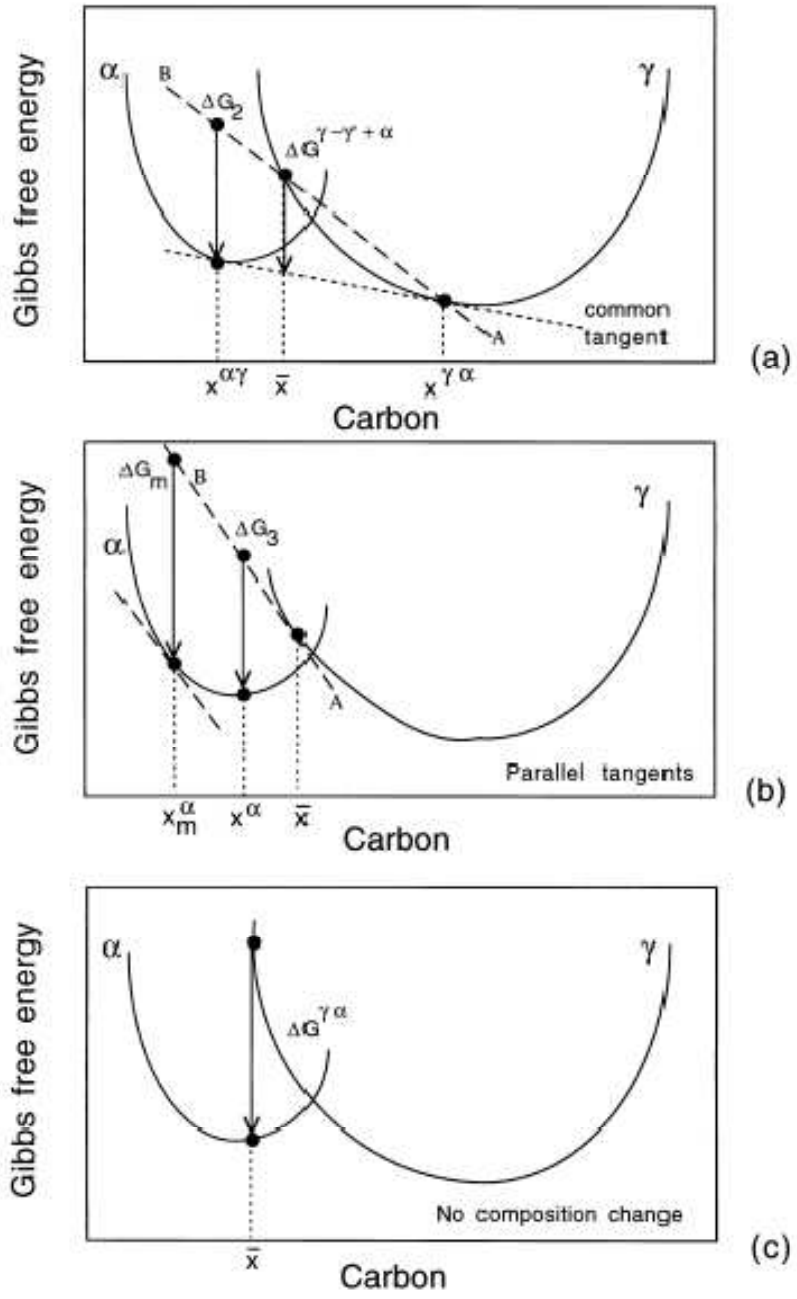

Fig. 1.7: Free energy diagrams illustrating the chemical free energy change during the nucleation and growth of ferrite from austenite of composition $\bar{x}$. The term *γ"* refers to austenite which is enriched in carbon as a result of the decomposition of austenite of composition $\bar{x}$ into a mixture of ferrite and austenite (Bhadeshia, 2001).

Time temperature transformation (TTT) diagrams consist essentially of two C-curves. The lower C-curve has a characteristic flat top at a temperature T_h, which is the highest temperature at which ferrite can form by displacive transformation (fig. 1.8). The transformation product at T_h may be Widmanstätten ferrite or bainite.

The analysis on driving forces at T_h gives information about nucleus of Widmanstätten ferrite and bainite. Analysis shown in fig. 1.9 proves that carbon must partition during the nucleation stage in order always to obtain a reduction in free energy. The situation illustrated in fig. 1.9b is not viable since diffusionless nucleation would in some cases lead to an increase in the free energy (Bhadeshia, 1981a).

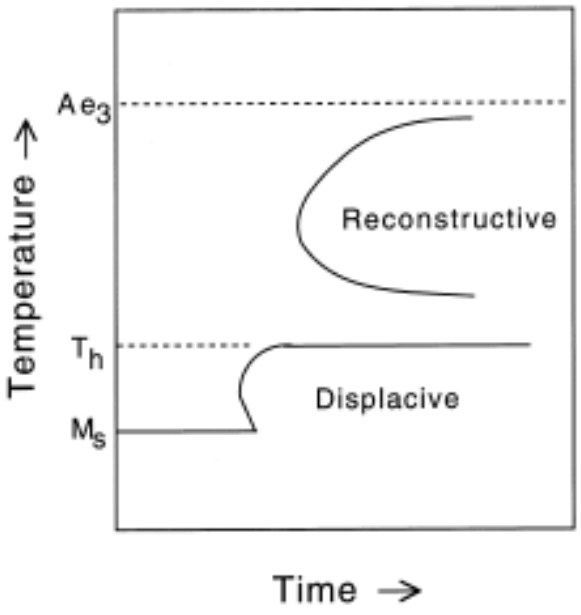

Fig. 1.8: Schematic TTT diagram illustrating the two C-curves and the T_h temperature (Bhadeshia, 2001).

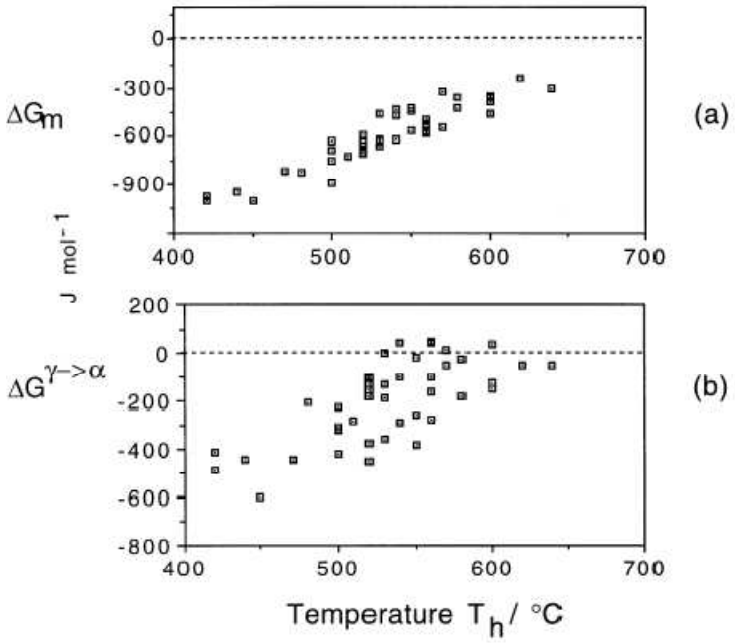

Fig. 1.9: The free energy change necessary in order to obtain a detectable degree of transformation. Each point represents different steel and there is no distinction made between Widmanstätten ferrite or bainite. (a) Calculated assuming the partitioning of carbon during nucleation. (b) Calculated assuming that there is no change in composition during nucleation (Bhadeshia 1981a).

The data in fig. 1.9 shows good linearity, the equation fitted to the data is (Ali and Bhadeshia, 1990)

$$G_N = C_1(T - 273.18) - C_2 \text{ J mol}^{-1} \quad (1.3)$$

where C_1 and C_2 are fitting constant. G_N is to be regarded as a *universal nucleation function*, because it defines the minimum driving force necessary to achieve a perceptible nucleation rate for Widmanstätten ferrite or bainite in any steel.

The nuclei of Widmanstätten ferrite and bainite are identical, but the thermodynamic condition determines whether the nucleus evolves into bainite or Widmanstätten ferrite. If diffusionless growth cannot be sustained at T_h then the nucleus develops into Widmanstätten ferrite so that T_h is identified with Widmanstätten ferrite start temperature (W_S). A larger undercooling is necessary

before bainite can be stimulated. If, however, the driving force at T_h is sufficient to account for diffusionless growth, then T_h=B_S and Widmanstätten ferrite does not form at all. The thermodynamic conditions for three displacive transformations can be summarised as table 1.2.

As shown in table 1.2, carbon diffusion in the bainite nucleation stage is one of the distinguishing features of bainite when compared with martensite. That's why carbon is effective to maintain the difference between M_S and B_S and high-carbon alloys were used for super-bainite. The above knowledge can be applied to predict transformation temperatures (Bhadeshia, 1981a; 1981b; 1981c; Ghosh and Olson, 2001; Garcia and Bhadeshia, 2004). Widmanstätten ferrite forms below the A_{e3} temperature when:

$$\begin{aligned} \Delta G^{\gamma\rightarrow\gamma'+\alpha} &< -G_{SW} \\ \Delta G_m &< G_N \end{aligned} \tag{1.4}$$

where G_{SW} is the stored energy of Widmanstätten ferrite (about 50 J mol^{-1}). The first of these conditions ensures that the chemical free energy change exceeds the stored energy of the Widmanstätten ferrite, and the second that there is a detectable nucleation rate.

	Nucleation (Mechanism, driving force)	Growth (Mechanism, driving force)
Widmanstätten α	Para-equilibrium, ΔG_m	Para-equilibrium, $\Delta G^{\gamma\rightarrow\gamma'+\alpha}$
Bainite	Para-equilibrium, ΔG_m	Diffusionless, $\Delta G^{\gamma\rightarrow\alpha}$
Martensite	Diffusionless, $\Delta G^{\gamma\rightarrow\alpha}$	Diffusionless, $\Delta G^{\gamma\rightarrow\alpha}$

Table 1.2: Summary of displacive transformations.

Bainite is expected below the T'_0 temperature when

$$\Delta G^{\gamma\rightarrow\alpha} < -G_{SB}$$
$$\Delta G_m < G_N \quad (1.5)$$

where G_{SB} is the stored energy of bainite (about 400 J mol^{-1}). Martensite forms when:

$$\Delta G^{\gamma\rightarrow\alpha} < G_N^{\alpha'} \quad (1.6)$$

where $G_N^{\alpha'}$ is the critical driving force needed to stimulate martensite by an athermal, diffusionless nucleation and growth mechanism. Whereas it is reasonable to set $G_N^{\alpha'}$ to a constant value for low alloy steels (Bhadeshia, 1981b; 1981c) a function dependent on the strength of the austenite has to be used for steels containing large concentrations of solute (Ghosh and Olson, 1994).

High-carbon alloys were used to develop super-bainite about 1 wt%. There is no lower limit to the bainite-start temperature, but it should be higher than M_S. The theory calculates the effect of carbon on transformation temperatures. Carbon is an element which very effectively depresses M_S and increases the gap between M_S and B_S as shown in fig. 1.10.

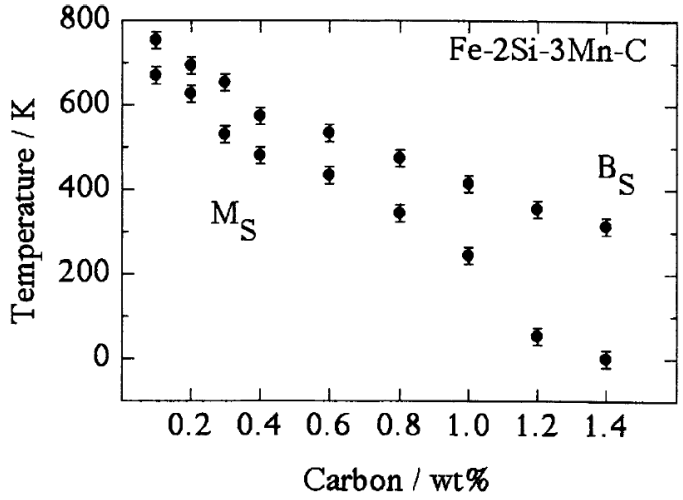

Fig. 1.10: Calculated transformation temperatures as a function of the carbon concentration (Garcia *et al*., 2003c).

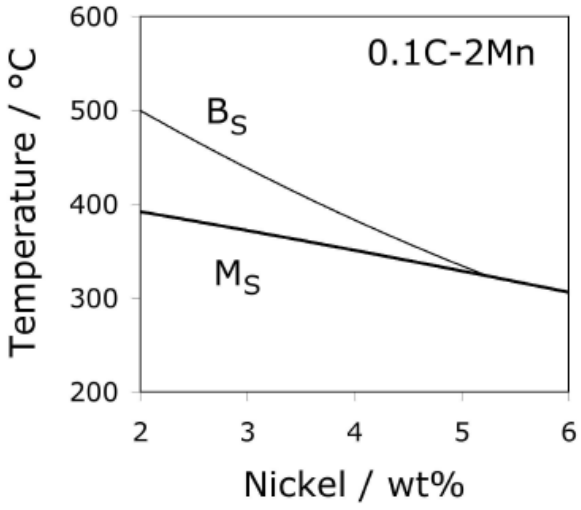

Fig. 1.11: Calculated bainite and martensite-start temperatures (Bhadeshia, 2006a).

It's useful to see transformation temperature variation as a function of substitutional element for examine possibility of low-carbon super-bainite. It's shown in fig. 1.11. The calculation shows that there would be a merge of M_S and B_S when nickel exceeds 5 wt %. A computer program which predicts M_S and B_S is available in the internet (Bhadeshia, 1987).

The aim of the work is to examine the calculation in fig. 1.11 experimentally and the possibility of low-carbon super-bainite. Alloys which contain 4-6 Ni wt % were made and tested to see weather the merger of B_S and M_S occurs or not.

1.5 Summary

Bainite grows by a sub-unit, displacive mechanism with an accompanying invariant-plane strain. Dislocations formed during plastic relaxation hinder the movement of the austenite/bainite interface. A bainite sub-unit can be thinner when austenite is strong, which means extremely fine scale microstructures are formed at low temperatures.

High-carbon alloyed bainitic steels which transformed at temperatures as low as 125-200 ℃ have a microstructure which is a mixture of very thin bainitic ferrite plates and retained austenite films. Its high strength and ductility combination has good potential for application in industry. Super-bainite does not require rapid cooling, which makes it possible in large scale with cheap price. However, high-carbon causes brittle martensite formation during welding. It is needed to develop low-carbon super-bainite. Theory predicts that low-carbon low-temperature bainite is impossible. This work was done to study the calculation and possibility of low-carbon super-bainite.

Ⅱ. Experimental

2.1. Alloy Production

A technique usually applied to manufacture standards for chemical analysis was used to make the alloys. Solid cylindrical samples of dimensions 3.6×8 cm were centrifugally cast and then homogenised in a vacuum furnace for 2 days at 1200 ℃. Three alloys were made to verify the calculation (fig. 1.10), namely 4Ni, 5Ni and 6Ni alloys. The length of the samples was then cut into several pieces of equal thickness; their individual chemical analyses are shown in Table 3.1. The carbon concentration was analysed using a LECO analyser to a reproducibility of ±0.0013 wt %, and the remaining elements using spark optical emission spectroscopy to a reproducibility of ±0.003 wt %. As shown in Table 3.1, the samples are well homogenized, so that all pieces of each alloy were treated as if they have the same composition.

Designation	**4Ni alloy**			**5Ni alloy**			**6Ni alloy**		
Sample	Mn	Ni	C	Mn	Ni	C	Mn	Ni	C
1	2.28	4.04	0.132	2.26	5.02	0.124	2.51	6.72	0.203
2	2.28	4.04	0.132	2.28	5.03	0.126	2.51	6.74	0.203
3	2.28	4.03	0.130	2.26	5.01	0.126	2.48	6.71	0.201
4	2.25	4.02	0.132	2.28	5.05	0.126	2.51	6.77	0.201
5	2.28	4.03	0.130	2.24	4.97	0.123	2.51	6.75	0.202
6	2.28	4.04	0.132	2.28	5.04	0.127			
Average	**2.275**	**4.033**	**0.1313**	**2.27**	**5.02**	**0.125**	**2.50**	**6.74**	**0.202**

Table 2.1: Chemical compositions in wt %

2.2 Dilatometry

2.2.1 Quenching Experiments (Measuring M_S)

Dilatometric samples were machined by spark erosion, in the form of cylinder of diameter 4 mm and length 7 mm, some of which were made hollow by drilling a 3 mm diameter longitudinal hole. A push rod *BAHR DIL805* high speed dilatometer with radio frequency induction was used. The sample temperature is measured by a thermocouple welded to its surface using a precision welder and jig supplied by the dilatometer manufacturer.

Each sample was austenitised at 950 ℃ for 3 min, followed by cooling at a constant rate to ambient temperature. The cooling rates used were in the range 3.2–330 ℃ s^{-1}. It was not possible to maintain a constant cooling rate when $|\dot{T}| \geq 140$ ℃ s^{-1}, so the stated values in those cases are over the range 300–500 ℃. The heating rate used was 30 ℃ s^{-1}. The heating and austenitisation treatments were carried out under a vacuum of 5×10^{-4} mbar, and the cooling was achieved using helium or argon gas.

2.2.2 Isothermal Experiments

Samples were austenitised at 950 ℃ for 5 min, followed by quenching to isothermal temperature. Samples were kept at constant temperatures for from 1 h to 30 h according to the transformation kinetics. After isothermal heat treatment, they were quenched at about 50-30 ℃ s^{-1}.

2.3 Transmission Electron Microscopy

Samples for transmission electron microscopy were prepared from 300 μm thick samples which were then reduced in thickness from both sides using SiC paper to a thickness of about 80 μm before punching out 3 mm discs. These foils were electropolished at room temperature, until perforation occurred, using a *Tenupol*-5 polisher set at 20-40 V. The electrolyte consisted of 6-8 % perchloric acid and 92-94 %

acetic acid. The thin foils were examined in a *Philips CM*200 transmission electron microscope operated at 200 kV.

2.4 Optical Microscopy

Samples for optical microscopy were etched using a 3 % Nital or a solution of 1 g sodium metabisulfite in 100 mℓ water mixed with 4 g of picric acid dissolved in 100 mℓ of water, for 1-30 sec (LePERA, 1979; Lawson *et al*., 1980).

2.5 X-ray Diffraction

Samples after isothermal experiments were polished using SiC paper. They were analyzed by *BRUKER D8* X-ray diffractometer. Beams were step scanned at speed of 0.1 degree per minute using Cu K_α X-ray.

2.6 Hardness Tests

Vickers hardness tests were carried out with a load of 2 kg for 10 sec duration.

Ⅲ. Martensite Start Temperatures

3.1 Uncertainties in Dilatometric Determination of M_S

There is a change in density when martensite forms in steels, which can be measured using dilatometry (fig. 3.1). Most dilatometers are of the push-rod type and hence are limited to detecting the length change due to the volume strain accompanying solid state reactions.

One of the parameters that can be detected from that expected due to the thermal contraction is taken to imply transformation. This raises difficulties in that the extent of deviation must be defined and the procedure used in not always clear. Chupatanakul and Nash (2006) identified lower the point where the curve departs significantly from thermal contraction at a temperature (fig. 3.2). Even for the case where the definition of M_S is the point where expansion is detected, uncertainties exist because the output of a dilatometer is never perfect (fig. 3.3); the data contain noise which is mostly ignored when measurements are reported.

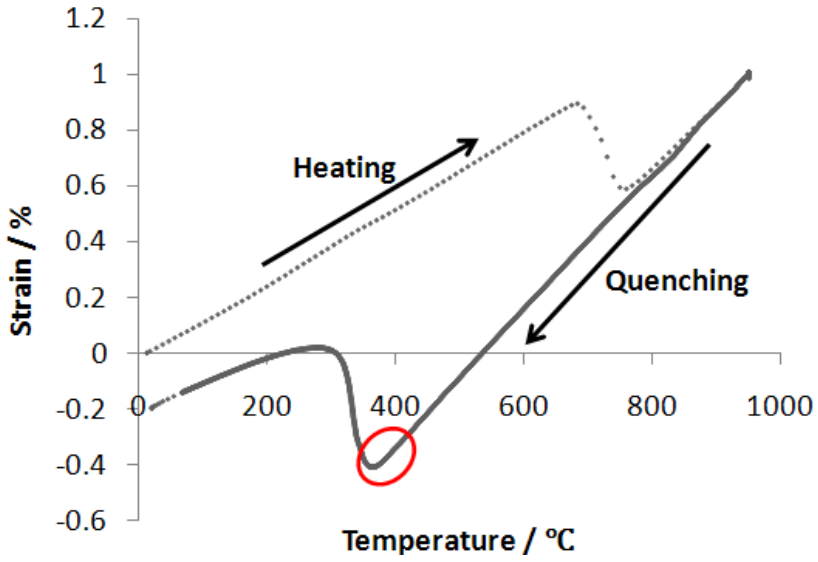

Fig. 3.1: Typical dilatometric data for M_S determination. M_S is roughly around the circled temperature. The quenching region looks continuous because a lot of data were recorded.

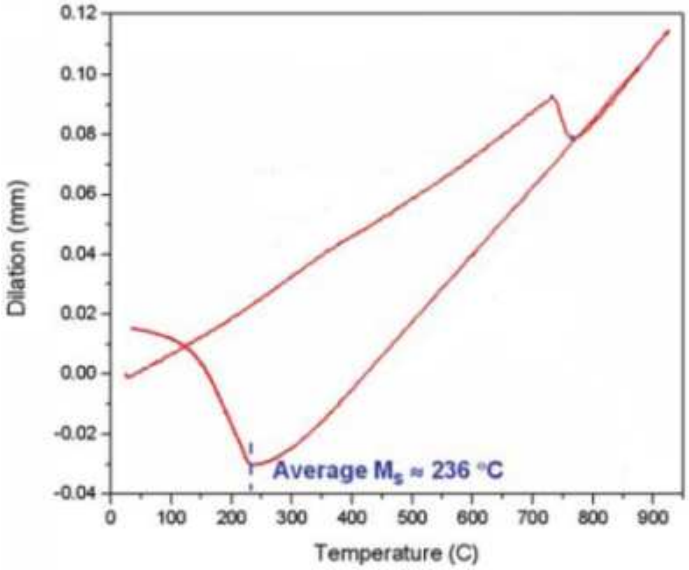

Fig. 3.2: Chupatanakul and Nash (2006) identified M_S as the minimum of the data, which is wrong. M_S should actually be higher, where line starts to be curved.

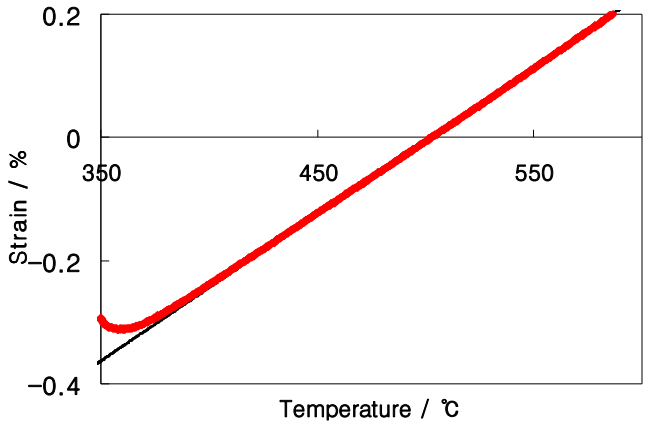

Fig. 3.3: Linear line is trend line to austenite linear contraction. M_S where strain data departs from contraction line is not clear. Austenite contraction region is almost straight.

In order to avoid such difficulties, the effect of this noise on the determination of the M_S temperature was examined systematically and offset method (described later) was chosen as the best method to measure the M_S (Yang and Bhadeshia, 2007). The method enables independent assessments of the same dilatometric data to reach identical numerical conclusions.

Among 3 alloys, 4Ni alloy was used to study the uncertainties in dilatometric M_S. Samples were heated to 950 ℃ at the rate of 30 ℃ s^{-1}, giving A_{C1} and A_{C3} temperatures of 652 and 751 ℃ and austenitised for 3 min, followed by quenching. A_{C1} and A_{C3} are temperature where $\alpha \rightarrow \gamma$ transformation starts and finishes respectively. Pieces of the alloy have a small difference in composition, and its actual composition data can be used to estimate the expected variation in the martensite-start temperature. Using the methodology described elsewhere (Bhadeshia, 1981b; 1981c) the variation expected on the basis of the compositions is estimated to be just ± 1 ℃.

For the sample size used, the resolution of the BHAR dilatometer is 50 nm, corresponding to a strain of 7.1×10^{-6} and a martensite volume fraction of 1.1×10^{-3} at 400 ℃.

The full set of experimental measurements is recorded in Table 3.1 for subsequent discussion.

Sample	$\lvert\dot{T}\rvert$, ℃ s^{-1}	Expansion Method M_S, ℃			Offset Method M_S, ℃
		Lower	Upper	Mean	*ε=1.21×10^{-4}
4, solid	3.2	439	470	455	377
4, solid	5.3	440	504	472	376
4, solid	7.9	420	448	434	363
5, solid	15.8	441	512	477	372
4, solid	15.8	385	412	399	358
5, solid	63.3	435	529	482	363
3, solid	140	379	395	387	361
3, hollow	31.7	444	504	474	401
3, hollow	47.5	441	494	468	392
1, hollow	95	375	383	379	366
3, hollow	95	378	390	384	372
3, hollow	95	423	524	474	370
3, hollow	330	403	409	426	385
2, hollow	330	393	-	-	375
3, hollow	330	-	-	-	374
3, hollow	330	367	372	370	365
Mean		411	456	434	373
σ		29	57	43	12

Table 3.1: Martensite-start temperatures as function of technique, for solid and hollow samples. The sample numbers in the first column correspond to those in 4Ni alloy of Table 2.1; σ is the standard deviation and $\lvert\dot{T}\rvert$ the cooling rate. *1.21×10^{-4} strain corresponds to 1 vol. % martensite assuming transformation at room temperature.

3.1.1. Detection of expansion

The thermal expansion coefficient of austenite, determined over the temperature range 420–650 ℃ was found in 16 separate experiments to be constant, with correlation coefficients in the range 0.99994–0.99999 in the plot of thermal strain versus temperature. It is reasonable therefore to assume that the austenite contracts linearly as the temperature is reduced (fig. 3.3). The thermal expansion coefficient of austenite from these experiments was found to be $2.43\times10^{-5} \pm 0.13\times10^{-5}$ ℃$^{-1}$, where the error is a single standard deviation.

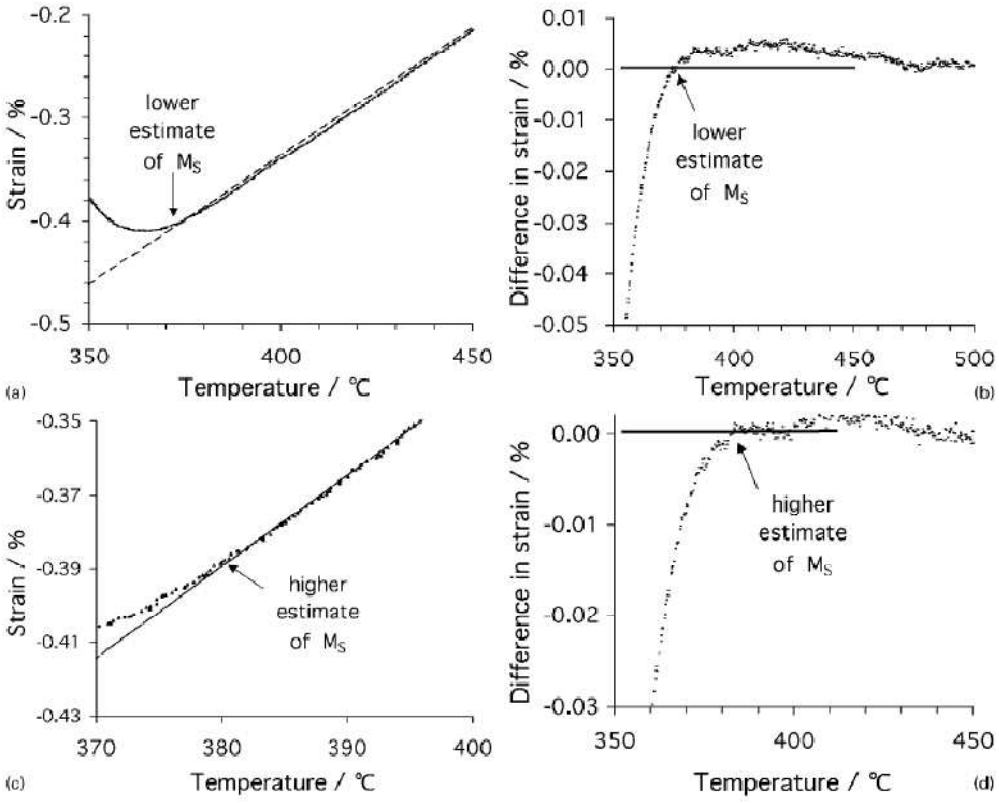

Fig. 3.4: Analysis of dilatometric data for hollow sample 1 cooled at 95 ℃ s^{-1}: Table 3.1. (a) lower bound of M_S temperature using (m+ Δm, C + ΔC); (b) as (a), but difference between fitted line and experimental data plotted on ordinate; (c) upper bound of M_S temperature using (m - Δm, C - ΔC); (d) as (c), but the difference between fitted line and experimental data plotted on ordinate.

It is common to take the first onset of expansion during cooling to correspond to the start temperature, but it is necessary to take account of noise. The root mean square level of noise in fitting a straight line to the thermal contraction of austenite was determined experimentally to be equivalent to a strain ε of $\pm 1.65\times10^{-5}$ which is greater than the resolution of the equipment (7.1×10^{-6}).

The expansion method relies on the detection of a deviation from the linear thermal contraction curve of austenite. This latter curve can be fixed by fitting a linear regression line to the data, yielding a slope m and an intercept C

$$\epsilon_\gamma = mT + C \tag{3.1}$$

where ϵ_γ is the measured strain as the austenite cools and T is the temperature. However, the slope and intercept are associated with standard errors, so four lines can be plotted ($m \pm \Delta m$, $C \pm \Delta C$), defining the upper and lower 95 % confidence limits to the austenite contraction curve.

Fig. 3.4 illustrates how, using the lines ($m + \Delta m$, $C + \Delta C$) and ($m - \Delta m$, $C - \Delta C$), the upper and lower bound M_S values given in Table 3.1 were obtained. The uncertainty particularly in the upper estimate of M_S is large because the curvature of the dilatometer output in that region is small. For this reason it was not possible in some cases, using this method, to define the martensite start temperatures, which means it's too difficult to specify a point where line starts to depart from cooling curve. Two examples emphasising that this method is unlikely to give reliable and reproducible results are illustrated in Fig. 3.5. The situation did not improve at all when the lines ($m + \Delta m$, $C - \Delta C$) and ($m - \Delta m$, $C + \Delta C$) were used. A larger number of cases occurred in which clear solutions did not exist.

Finally, it is worth noting that taking the derivative of the strain versus temperature curve does not help improve the assessment of the dilatometric data. The derivative itself suffers from noise in the slope as is evident by differentiating equation (3.1), where the error Δm in the slope is retained. Furthermore, additional problems arise because the derivative has to be calculated from discrete, noisy data. This is illustrated in Fig. 3.6, where the horizontal line represents the expansion coefficient of austenite. Since the expansivity of ferrite in all but the invar steels is always

smaller (Laufman *et al*., 1963), M_S is defined by the point where the expansivity falls below that of the austenite.

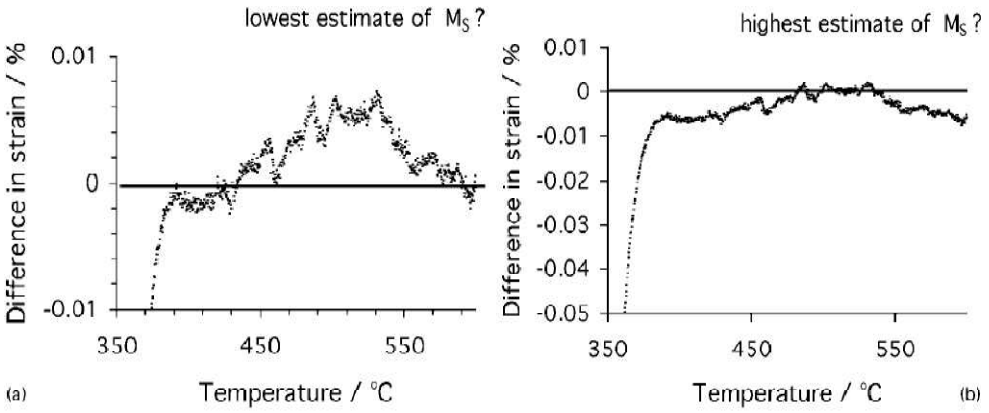

Fig. 3.5: Lack of clarity in determination of M_S: analysis of dilatometric data for hollow sample 3 cooled at 330 ℃ s^{-1}. (a) lower bound of M_S temperature using (m+ Δm, C + ΔC); (b) upper bound of M_S temperature using (m- Δm, C - ΔC)

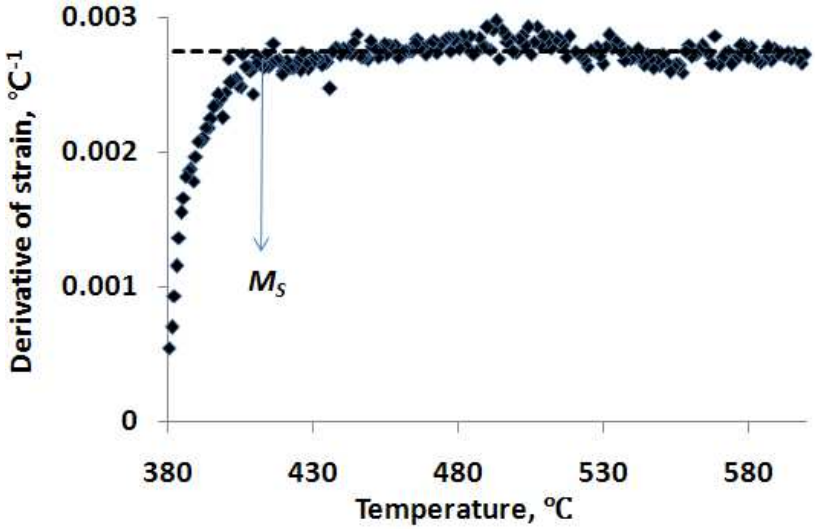

(a)

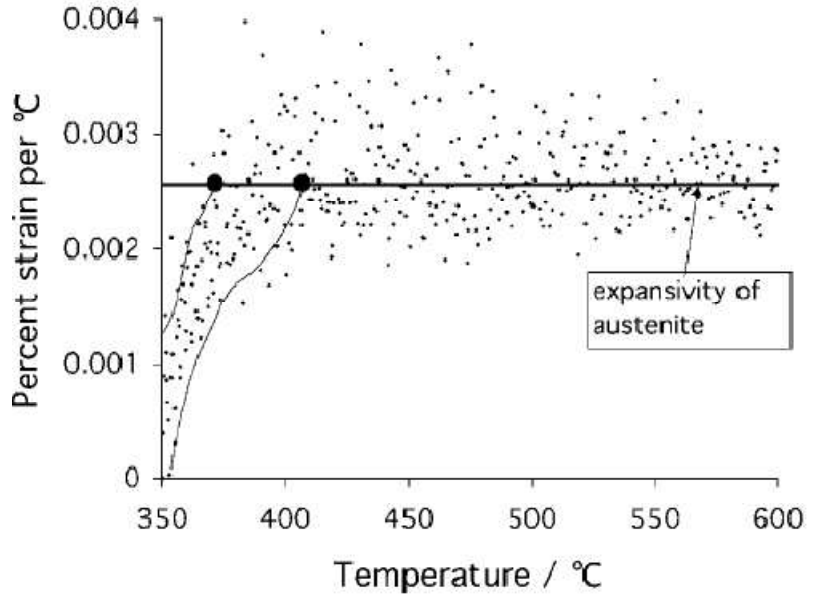

(b)

Fig. 3.6: Derivative of strain versus temperature dilatometric curve, plotted versus temperature. (a) One of the methods which uses derivatives of strain curve, this couldn't make reproducible analysis; each derivative is calculated from ten successive strain data (b) Two large points identify $\pm 1\,\sigma$ uncertainty in M_S and curves are polynomial fits to low temperature data, displaced by $\pm 1\,\sigma$ about best fit; each derivative is calculated from three successive strain data.

3.1.2 Offset Method

Offset method was used for determination of M_S in order to get reproducibility. The offset method is routinely used in defining the proof strength of materials when the stress–strain curve is smooth, making it difficult to define the deviation from elastic deformation. In the case of a tensile test, it is conventional to offset the test line by a strain of 0.2% in order to define the proof strength. A similar procedure could be followed for martensite as illustrated in fig. 3.7.

The question then arises as to the magnitude of the transformation strain that should be used as the offset from the thermal contraction curve of austenite in order to determine the martensite start temperature.

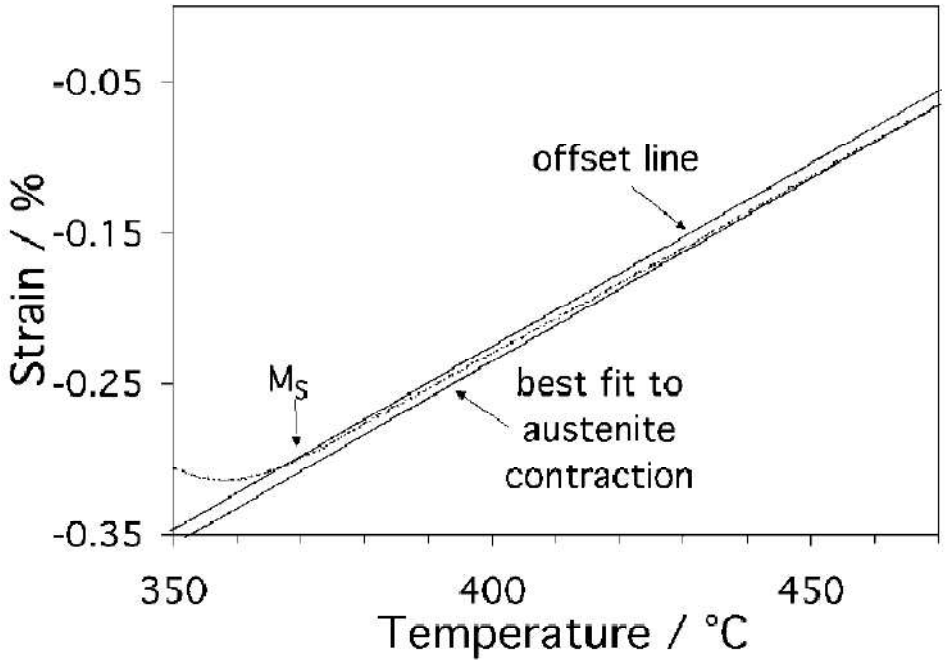

Fig. 3.7: Offset method illustrated. Best fit line moved up in order to make intersection clear.

A transformation strain due to 1 vol. % martensite can be set as the value of the offset at which M_S is measured. For the present steel, it will be shown that this corresponds to a strain of 1.21×10^{-4}, which is about ten times of the noise in the instrument and should be sufficient for the offset line to intersect the experimental curve in a region of sufficient curvature, thus ensuring a reliable measure of M_S.

The transformation strain depends of course on the alloy studied. The strain cannot be measured directly from the dilatometer curve since the martensite reaction may not reach completion at the point where the experiment is terminated. The critical strain corresponding to 1 vol. % martensite can be calculated if the lattice parameters a_γ and a_α of austenite and martensite respectively are known. The following equations are available from compiled data (Bhadeshia *et al*., 1991)

$$a_\alpha = 0.28664 + [(a_{Fe} - 0.0279\, x_C^\alpha)^2 (a_{Fe} - 0.2496\, x_C^\alpha) - a_{Fe}^3]/(3\, a_{Fe}^2) - 0.003 x_{Si}^\alpha + 0.006 x_{Mn}^\alpha + 0.007 x_{Ni}^\alpha + 0.031 x_{Mo}^\alpha + 0.005 x_{Cr}^\alpha + 0.0096 x_V^\alpha \quad (3.2)$$

where x_i^α represents the mole fraction of species i in phase α. The lattice parameter of pure iron a_{Fe} =0.28664 nm (US National Bureau of Standards, 1955). The equation applies at room temperature (25 ℃).

The parameter for austenite at room temperature is given by (Dyson and Holmes, 1970)

$$a_\gamma = 0.3573 + \sum_{i=1}^{n} c_i w_i^\gamma \quad (3.3)$$

where w_i represents weight fraction and

$$\sum_{i=1}^{n} c_i w_i^\gamma = 3.3 \times 10^{-1}\, w_C^\gamma + 9.5 \times 10^{-3} w_{Mn}^\gamma + 2 \times 10^{-3} w_{Ni}^\gamma + 6 \times 10^{-3} w_{Cr}^\gamma + 3.1 \times 10^{-2} w_{Mo}^\gamma + 1.8 \times 10^{-2} w_V^\gamma$$

Given that the austenite unit cell contains 4 iron atoms and that of martensite 2 per cell, the offset strain ε_0 corresponding to a specified value of martensite fraction V is given by

$$(1 + \varepsilon_0)^3 = a_\gamma^{-3} [2V a_\alpha^3 + (1 - V)\, a_\gamma^3] \quad (3.4)$$

The essence of the offset method is unlikely to be a new concept in the context of dilatometry. However, it is important to note that the method for calculating the

critical value ε_0 of the offset strain leads to an entirely reproducible value of M_S. The last column of Table 3.1 shows the results calculated in this way.

It is worth noting that the average value of the M_S temperature, measured using the offset method, changes from 419, 384, 382 to 373 ℃ as the volume percentage of martensite at which M_S is measured is changed from 0.08, 0.5, 0.54 and 1 vol.% respectively. Although this appears at first sight to be awkward, it is well established that the M_S temperature depends on the sensitivity of the technique used. Thus, acoustic emission can be much more sensitive than electrical resistivity measurements, so the M_S temperature measured using the latter technique is much lower than associated with acoustic data (Olson *et al*., 1987)

Consequently, in situations where it is important, it would be good practice to quote both the M_S temperature and the offset ε_0 used in its definition.

The offset method clearly is more reliable than the expansion method. This is also evident in Table 3.1 where the standard deviation of the measurements is smaller for the offset method with $\sigma = \pm 12$ ℃. It is useful to compare this with the noise perceived when large quantities of M_S data are analysed using a neural network method based on a Bayesian framework (Capdevila *et al*., 2002; 2003). One advantage of a Bayesian framework is that it avoids overfitting to the data and hence should give a reliable estimate of noise in the reported M_S values (Bhadeshia, 1999; Mackay, 2003). The perceived normalised noise in the M_S is $\sigma \cong \pm 0.04$. Taking the M_S temperature as 373 ℃, $\sigma \cong \pm 15$ ℃ is obtained. That this is larger than reported here for the offset method might be expected since the neural networks rely on large quantities of data compiled from diverse sources. In other neural network analyses not using a Bayesian framework, the standard error in the M_S was found to be ±15.3 ℃ (Wang *et al*., 2000) and ±12 ℃ (De Weijer *et al*., 1996).

In contrast, the standard deviation in the M_S data determined using the expansion method is unrealistically large at $\sigma \cong \pm 43$ ℃.

3.1.3 Source of the error

The equipment used in the present work has a much higher spatial resolution than the noise detected in the experimental data. A standard deviation of 12 ℃ in the M_S measurements using the offset method is large and as pointed out earlier, cannot be accounted for by variations in the chemical composition.

A contribution to the observed variations in M_S may arise from the fact that the samples do not achieve a uniform temperature during the experiments. Fig. 3.8 shows a comparison between the data for the solid and hollow samples. There is no systematic difference between the two kinds of specimens indicating that even the hollow samples may not achieve a sufficiently uniform temperature during cooling.

An additional explanation is that the early stages of martensitic transformation are sensitive to the initial austenite grain structure (Maki *et al*., 1971; Brofman and Ansell, 1983) in which case there is no guarantee that identical grain structures are generated in every sample. Martensitic nucleation can occur from arrays of dislocations associated with grain boundaries and therefore may be sensitive to the nature of those boundaries (Olson, 1976).

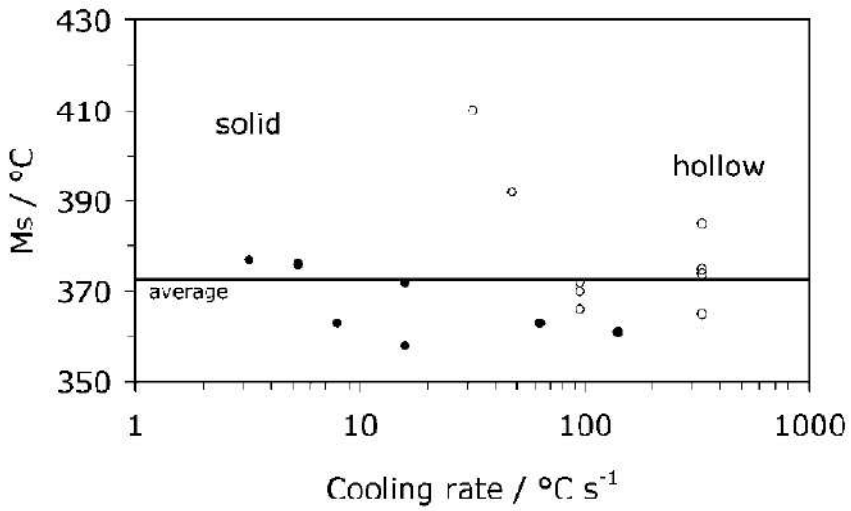

Fig. 3.8: M_S temperatures using offset method, for solid and hollow specimens as function of cooling rate.

3.1.4 Summary

A method is proposed in which dilatometric data are interpreted by defining the first onset of transformation to be that at which a critical strain is achieved relative to the thermal contraction of the parent phase. The critical strain is calculated for 1 vol. % martensitic transformation assuming that the latter occurs at room temperature, by using equations for the lattice parameters of austenite and martensite. This ensures that the method is reproducible and emphasises that transformation start temperatures should be quoted with the value of the critical strain used to interpret the dilatometric data.

3.2. Measured Martensite Start Temperatures

Offset method described in the previous chapter was used to determine the M_S of the samples. Strain corresponding to 1 vol.% martensite was used as offset. Typical dilatometric data are shown in fig. 3.9. At a glance, it's seen that 6Ni alloy has lowest M_S because 6Ni has higher nickel concentration. And critical reason is its higher carbon concentration which is not intended. All M_S data are presented in table 3.2.

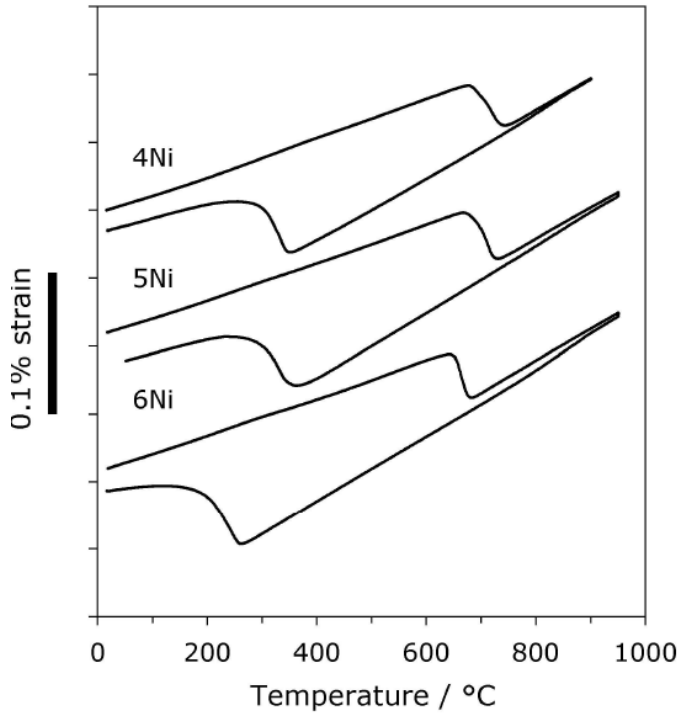

Fig. 3.9: Typical dilatometric data for martensite–start temperature determinations.

Alloy	Offset	M_S / ℃	Mean	Standard deviation
4Ni alloy	1.21×10^{-4}	377 376 363 372 358 363 361 401 392 366 372 370 385 375 365 -	373	12
5Ni alloy	1.24×10^{-4}	361 360 383 382 - - - -	372	13
6Ni alloy	1.30×10^{-4}	265 258 292 290 278 278 284 285 253 252 260 264 270 - - -	272	14

Table 3.2: Measured M_S temperatures. Offset corresponds to 1 vol. % martensite assuming transformed at room temperature.

Ⅳ. Low-Carbon Low-Temperature Bainite

4.1 Dilatometric Data

Dilatometry was used for isothermal heat-treatment. It enables a precise temperature to be set whilst the specimen is under vacuum, while at the same time allowing strains due to transformation to be continuously monitored. The 6Ni alloy requires a long time to achieve transformation and dilatometer is not designed for very long heat-treatments. The 6Ni alloy was therefore vacuum sealed, austenitised in the furnace and put into an oven at 280 ℃ for 12 weeks.

Dilatometric samples of each alloy were austenitised followed by quenching to the isothermal reaction temperature. They were kept at the temperature from between one and 30 h according to the transformation kinetics. Typical isothermal dilatometric data are shown in fig. 4.1. The expansion during isothermal holding is assumed to be due to bainitic transformation because experiments were started from a temperature slightly higher than M_S. There is another expansion during quenching to ambient temperature from the isothermal temperature, due to martensitic transformation of any remaining austenite. The temperature where martensitic transformation starts is higher than the M_S of the alloy because residual austenite becomes carbon-enriched by bainitic transformation. However, as will be shown later using X-ray analysis, the carbon-enrichment is not sufficient to stabilize the austenite at room temperature.

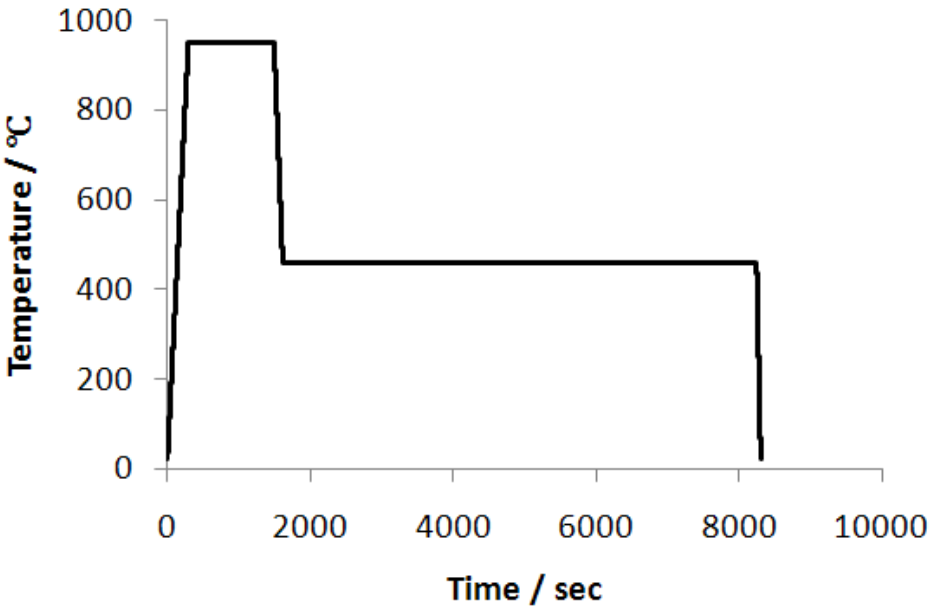

(a)

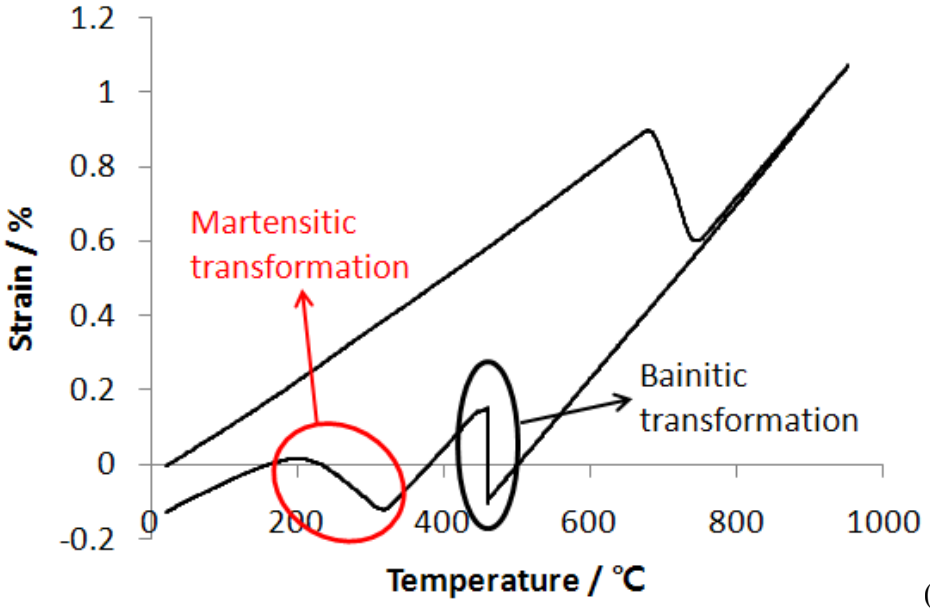

(b)

Fig. 4.1: 4Ni alloy, isothermally transformed at 460 ℃ for 100 min followed by quenching. The M_S is lower than that of the alloy. (a) temperature profile (b) strain versus temperature data

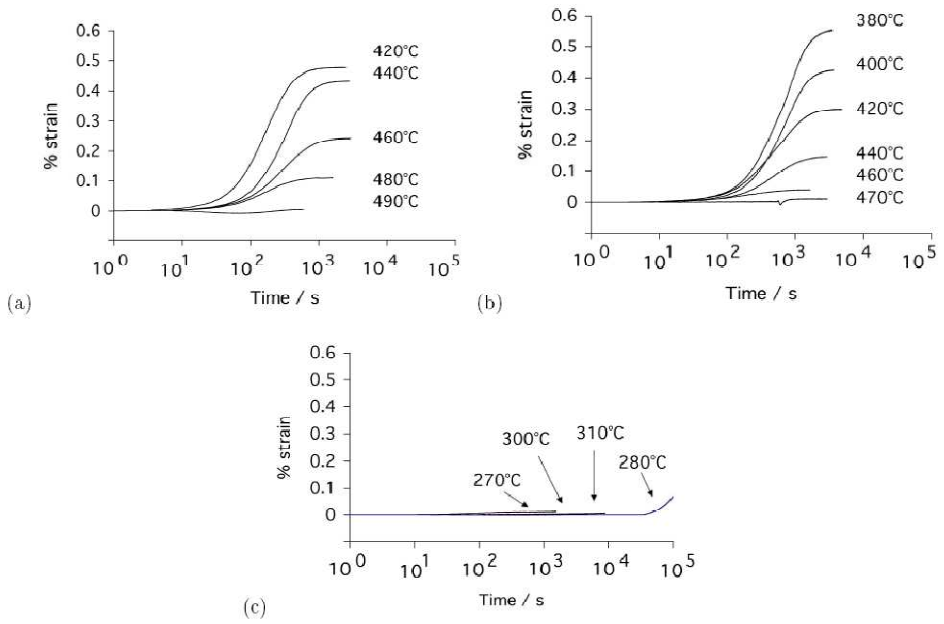

Fig. 4.2: Isothermal transformation dilatometric curves exploring the formation of bainite. (a) 4Ni alloy, (b) 5Ni alloy, (c) 6Ni alloy – in this figure, the end points of the experiments are marked for clarity.

The Isothermal parts of the dilatometric data are summarised in fig. 4.2. The kinetics of the 6Ni alloy were much slower than those of other alloys. It is just possible to see the initiation of the transformation at 280 ℃ in 30 h heat-treatment.

Fig. 4.2 shows that the bainite fraction reduces as the transformation temperature increases, and ultimately becomes zero at B_S in the 4Ni and 5Ni alloys. This can be explained using the T_0 concept. $\bar{x}$ is carbon concentration of the alloy. Assuming that the bainitic plates contain no carbon, the maximum bainite fraction V that can be formed at temperature T is given by (fig. 4.3):

$$V = \frac{(x_{T_0'} - \bar{x})}{x_{T_0'}} \tag{4.1}$$

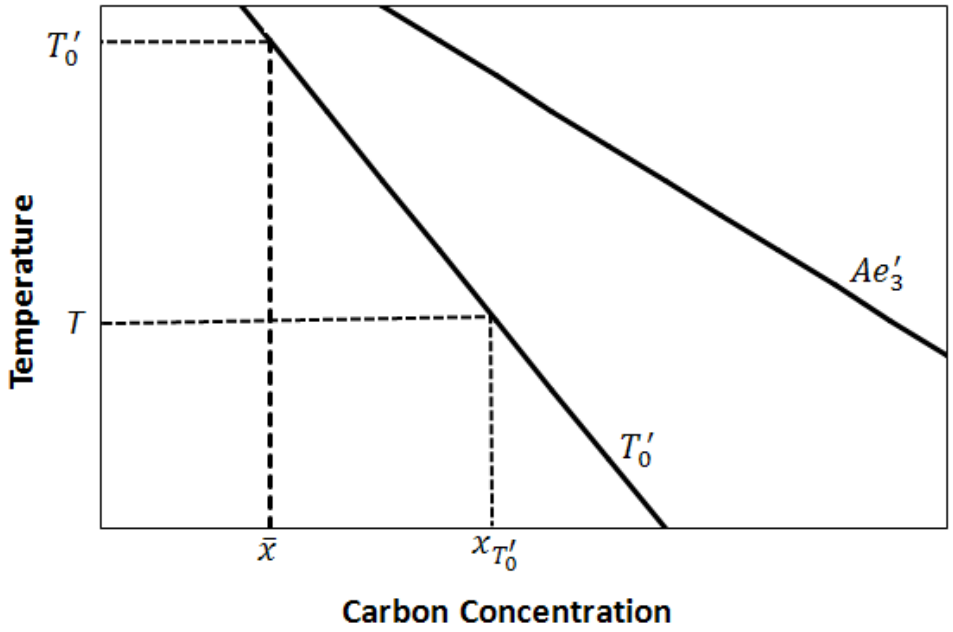

Fig. 4.3: Incomplete reaction phenomenon. After bainitic transformation, the residual austenite has a carbon composition given by the T_0' line rather than Ae_3'. Ae_3' refers to para-equilibrium (γ+α)/γ phase boundary.

Fig. 4.3 shows why the bainite fraction becomes smaller as the transformation temperature increases. It becomes zero at T_0', which means that B_S=T_0'. It seems that B_S=T_0' for the 4Ni and 5Ni alloys. As mentioned in chapter 1, two criteria should be satisfied for bainite to be possible. The first corresponds to the growth criterion that there must be sufficient free energy available to sustain diffusionless transformation together with a strain energy of some 400 J mol^{-1}. In other words, bainite can be formed when the temperature is below T_0'. The second is a nucleation condition in which the free energy change calculated allowing for carbon partitioning between the parent and product phases must exceed a value given by the universal nucleation state reference function. The nucleation criterion is redundant in the case of 4Ni and 5Ni alloys because the data show that the bainite fraction becomes smaller and finally becomes zero at B_S. If the nucleation criterion is not redundant, there would be a considerable amount of bainite formation at B_S because B_S would be below T_0'.

Fig. 4.3 and the T_0' concept lead to a further conclusion that there are no carbides precipitating and even if they exist, the quantity must be negligible. As mentioned in chapter 1, the incomplete reaction phenomenon is only applicable in the absence of carbide precipitation. If carbides are formed, austenite would not be enriched in carbon and would continue to transform until the microstructure is fully bainitic. Carbide formation can be detrimental to mechanical properties; it can be suppressed by silicon alloying. Super-bainite uses about 1.5 wt% silicon alloying to suppress carbides formation (Garcia-Mateo *et al*., 2003b). Silicon does harm the surface quality of steels and limits their use in galvanised products (Chang, 1999). The 4Ni and 5Ni alloys contain low-carbon concentrations, which results in the absence of cementite without the help of silicon. This could be advantageous in the design of low-carbon super-bainite.

4.2 Characterization of the Transformation

Comprehensive metallographic and characterization experiments were conducted on all the specimens in order to verify the conclusions extracted from the dilatometric data and to examine the bainite.

Optical and transmission electron microscopy experiments were conducted in order to verify the occurrence of bainite and martensite in the three alloys. X-ray diffraction was performed to check again whether some austenite was retained. Vickers hardness test was applied to see whether it is consistent with the conclusion extracted from dilatometric and metallographic data.

4.2.1 Optical Microscopy

Every sample was examined using optical microscopy. The complete set of optical and transmission electron microscopy data are available elsewhere for examination[1]. The data are consistent with the dilatometry. It's easily seen that microstructures consist of bainite and martensite and that the bainite fraction reduces as temperature increases. Fig. 4.4 shows optical micrographs of the 4Ni alloy.

[1] http://cml.postech.ac.kr/2007/Ni/Ni.html

(a) 4Ni alloy. Quenched sample for reference. Fully martensitic.

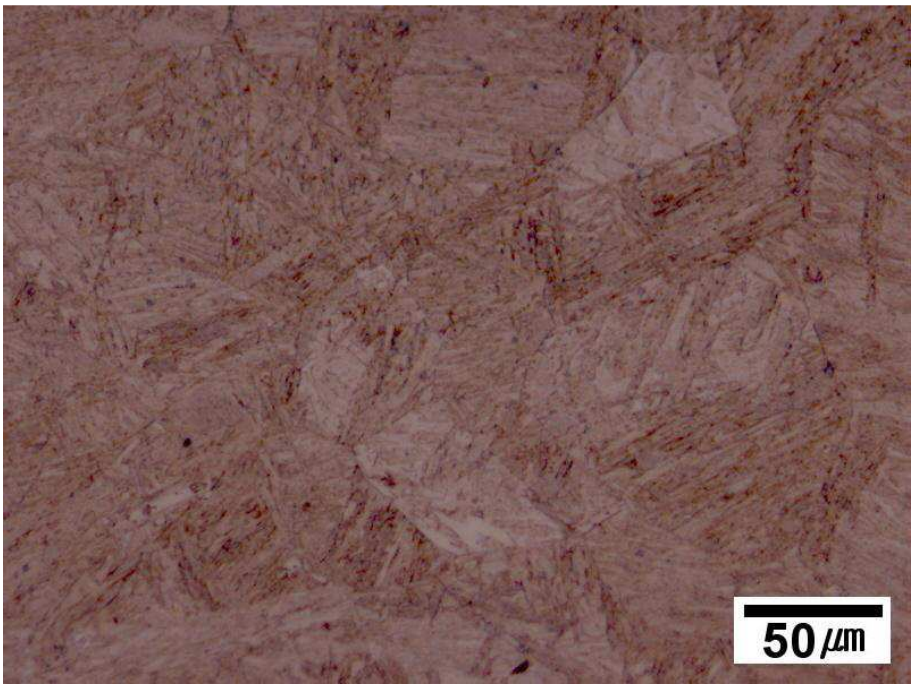

(b) 4Ni alloy. Isothermally transformed at 490 ℃. No bainite formed, fully martensitic.

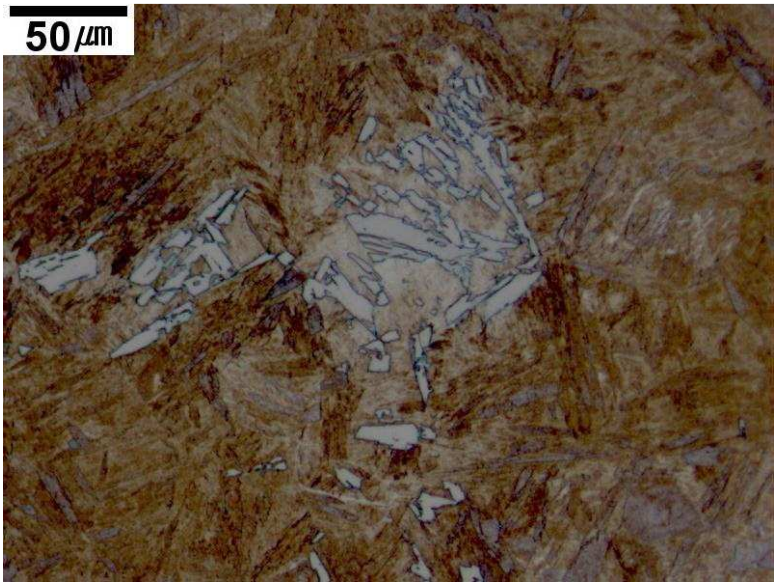

(b) 4Ni alloy. Isothermally transformed at 480 ℃. The white regions are bainite, the brown regions are martensitic. A small quantity of bainite was formed. The bainitic plates look quite thick, but they are not the individual plates. Individual plates are seen in TEM, as will be shown later.

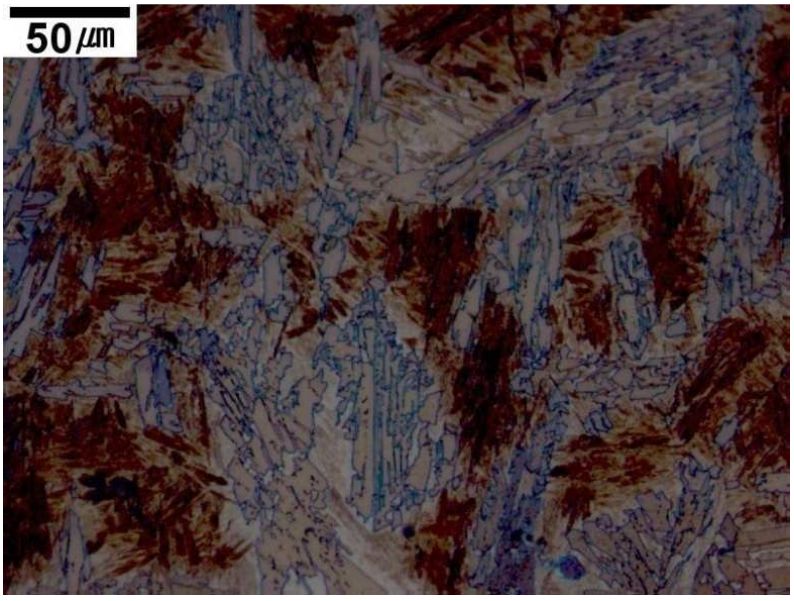

(d) 4Ni alloy. Isothermally transformed at 460 ℃. More bainite was formed than the sample transformed at 480 ℃.

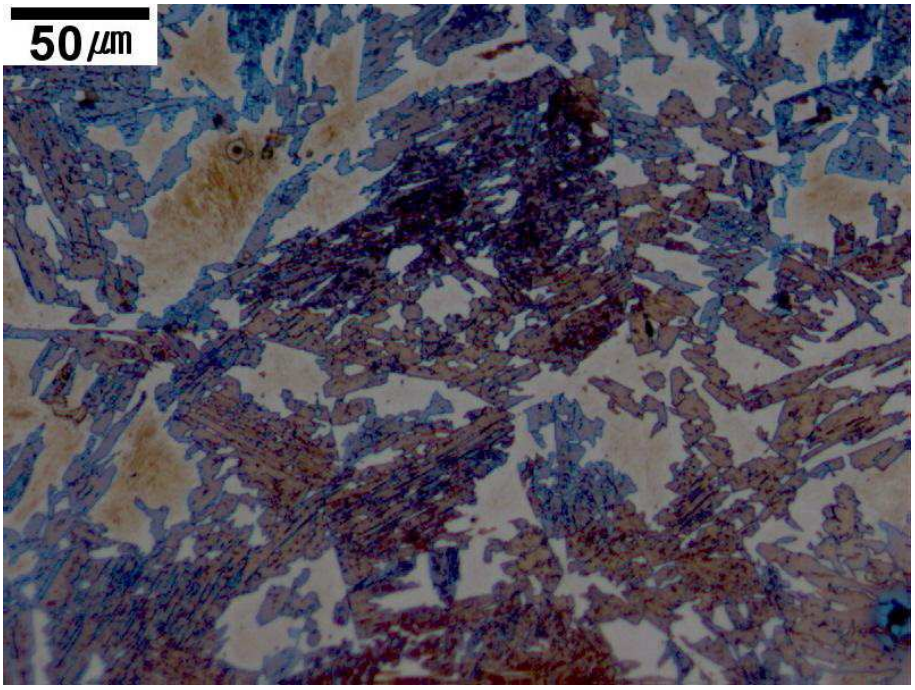

(e) 4Ni alloy. Isothermally transformed at 440 ℃. The light brown regions are martensitic. A lot of bainite is evident.

Fig. 4.4: Optical micrographs of the 4Ni alloy.

Micrographs of the 5Ni alloy also show consistent results with dilatometric data (Fig. 4.5).

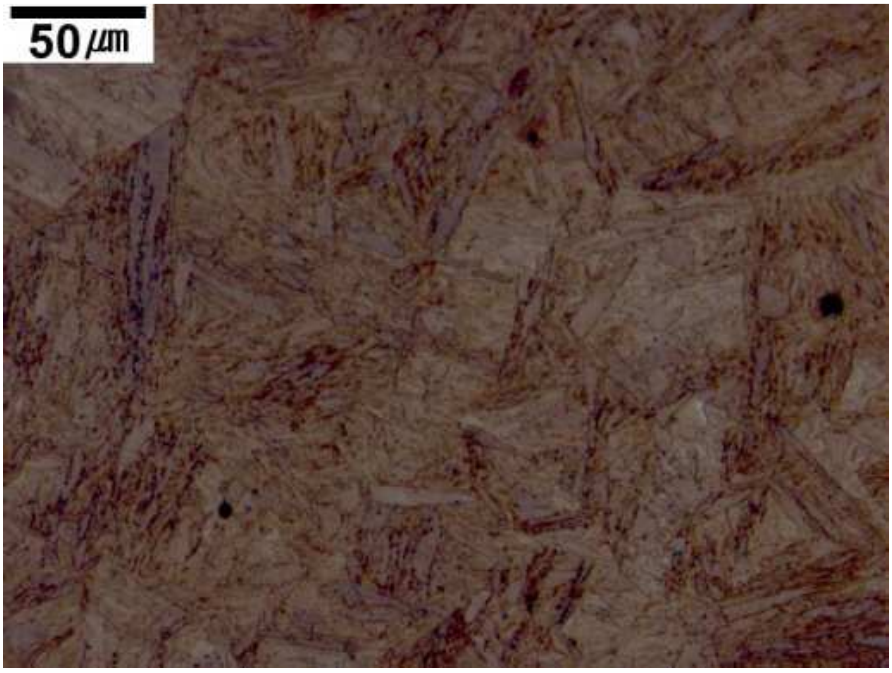

(a) 5Ni alloy. Quenched sample for reference. Fully martensitic.

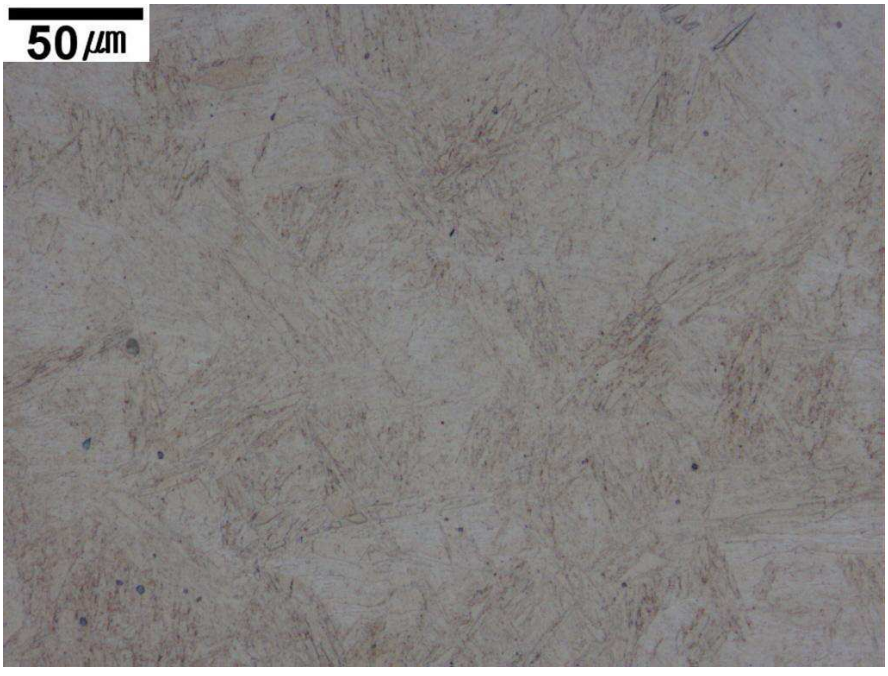

(b) 5Ni alloy. Isothermally transformed at 470 ℃. No bainite formed, fully martensitic.

(c) 5Ni alloy. Isothermally transformed at 460 ℃. Small fraction of bainite was formed.

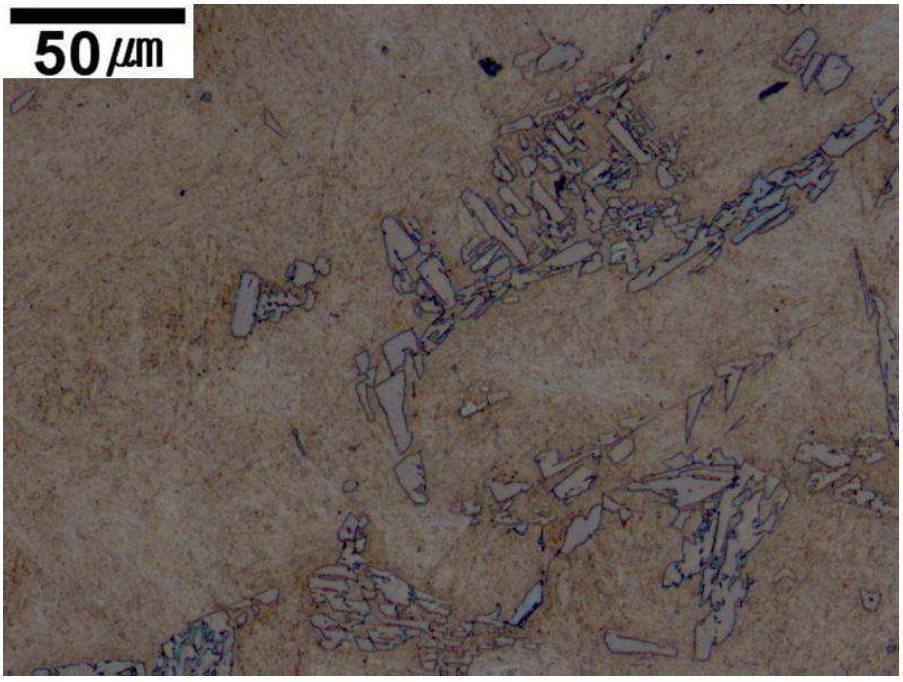

(d) 5Ni alloy. Isothermally transformed at 440 ℃.

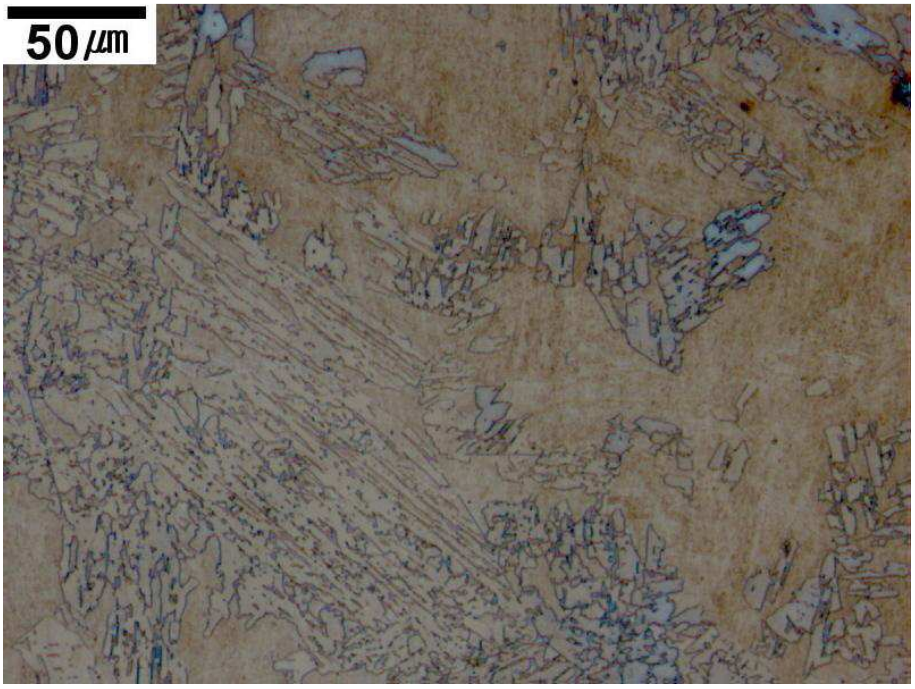

(e) 5Ni alloy. Isothermally transformed at 420 ℃.

Fig. 4.5: Optical micrographs of the 5Ni alloy.

Only the onset of the transformation in 6Ni alloy was seen using dilatometry. Prolonged heat-treatment at 280 ℃ was conducted and the micrographs in fig. 4.6 show the microstructures. As shown in fig. 4.2, it requires about 12 h before starting bainitic transformation. Consistent with that, there is no bainite before 12 h of heat-treatment. The bainite fraction increases as time passes.

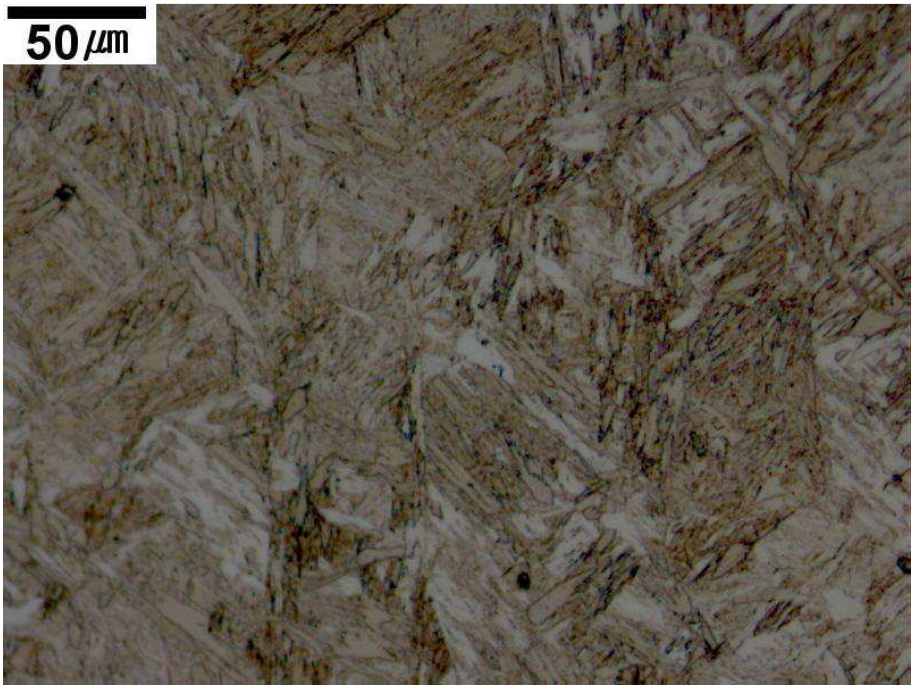

(a) 6Ni alloy. Austenitised followed by quenching. Fully martensitic.

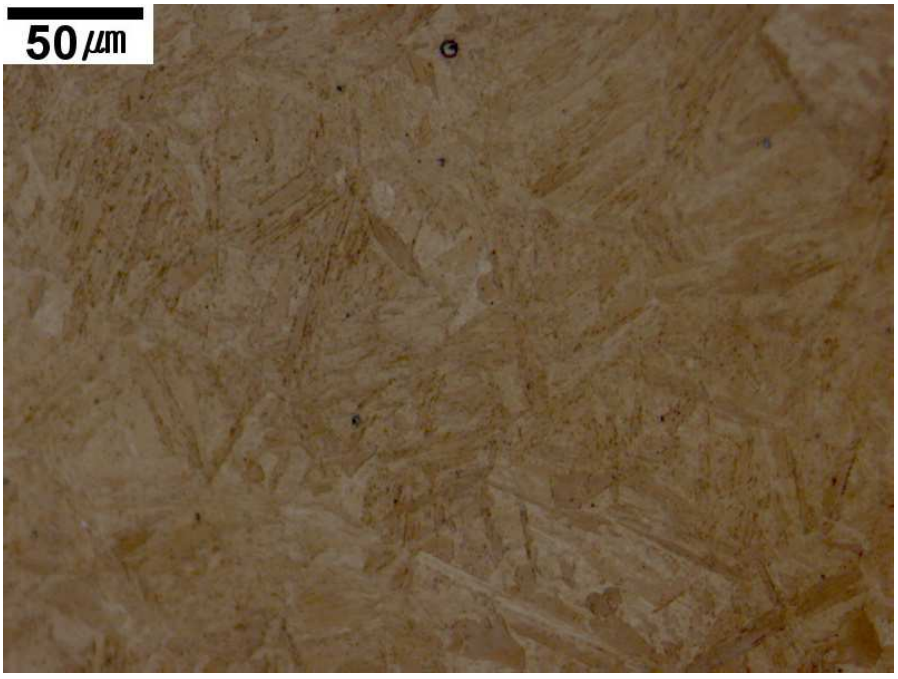

(b) 6Ni alloy. Isothermally transformed at 310 ℃ for 3 h. No bainite, fully martensitic.

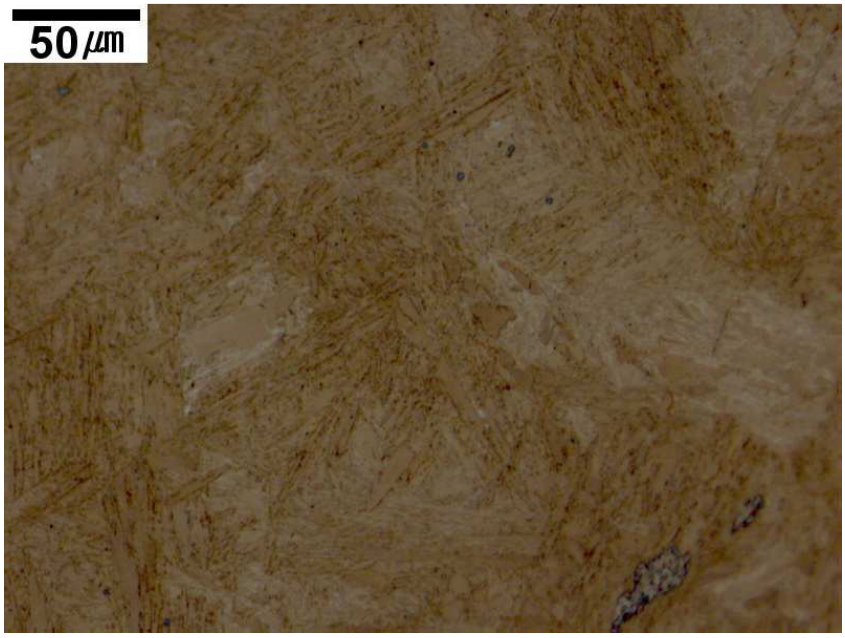

(c) 6Ni alloy. Isothermally transformed at 300 ℃ for an hour. No bainite, fully martensitic.

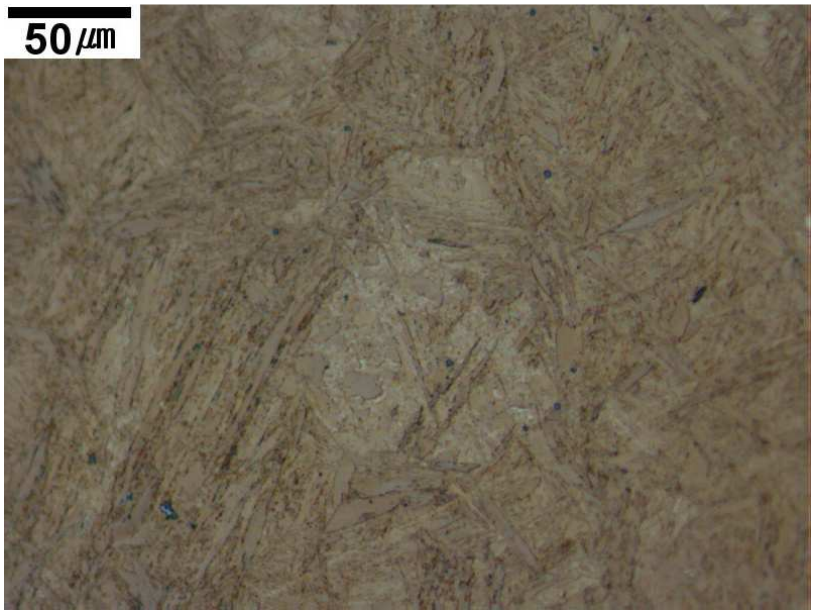

(d) 6Ni alloy. Isothermally transformed at 280 ℃ for 6 h. Bainite transformation not started yet, fully martensitic.

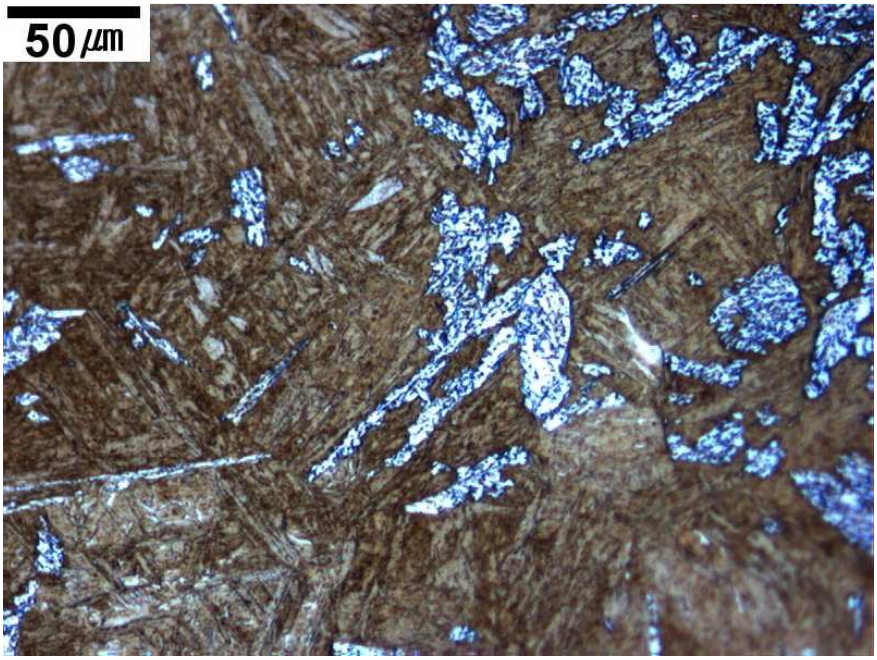

(e) 6Ni alloy. Isothermally transformed at 280 ℃ for 30 h. Bainitic transformation started. A small quantity of bainite is seen.

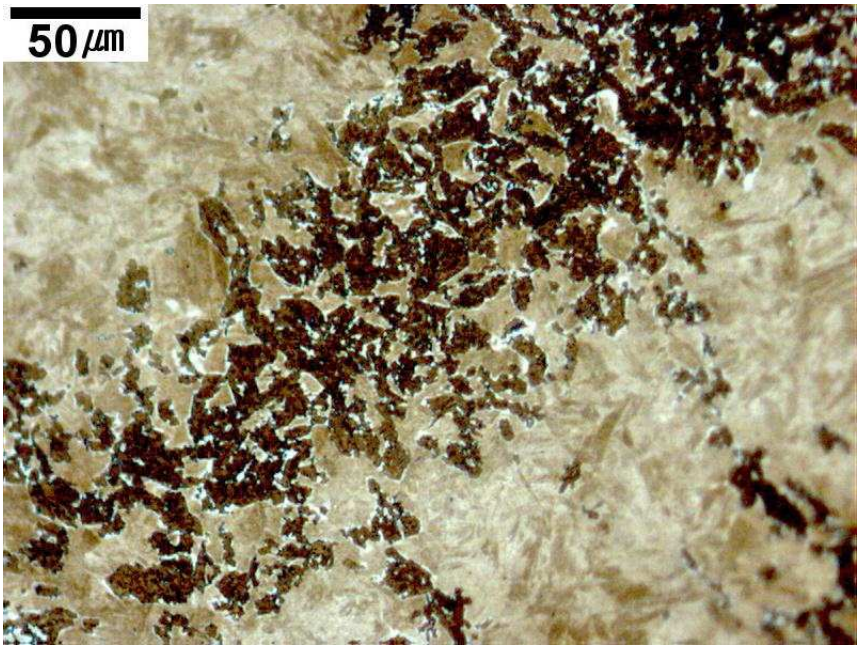

(f) 6Ni alloy. Isothermally transformed at 280 ℃ for 7 days.

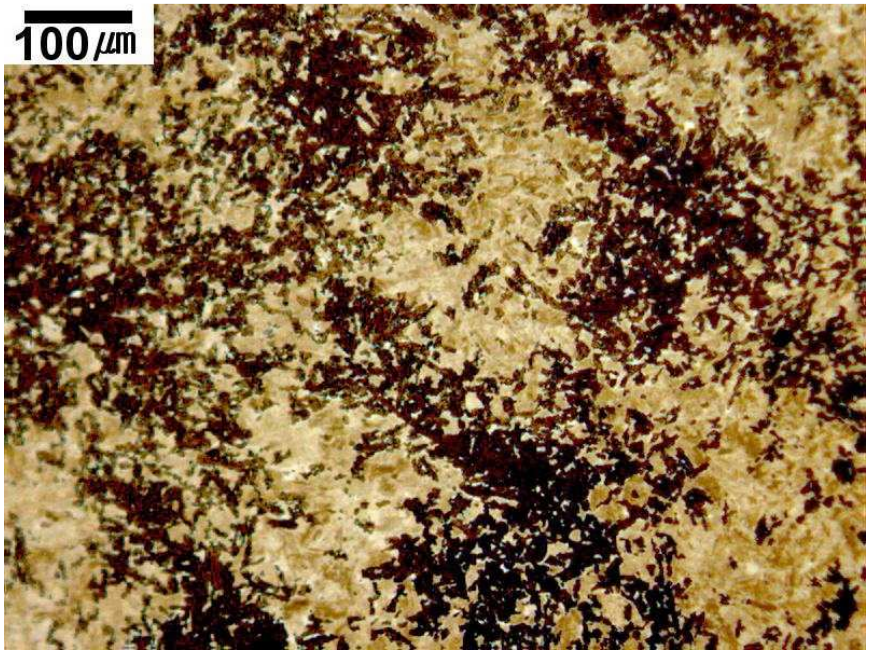

(g) 6Ni alloy. Isothermally transformed at 280 ℃ for 3 weeks.

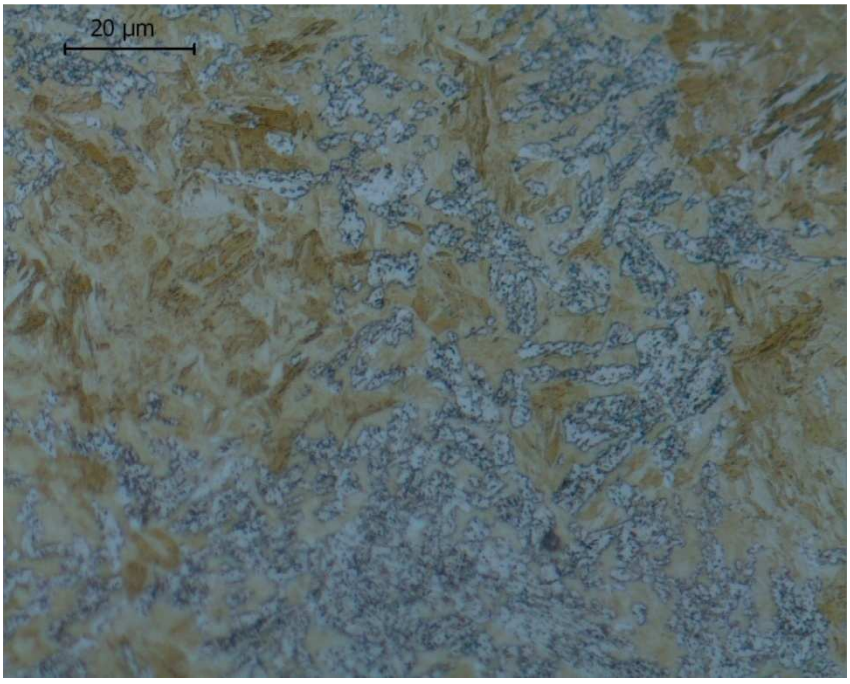

(f) 6Ni alloy. Isothermally transformed at 280 ℃ for 9 weeks.

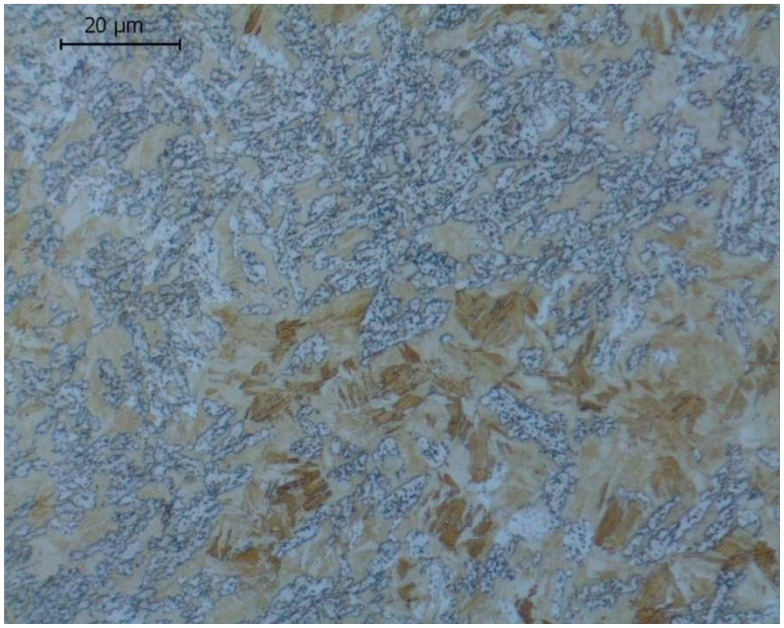

(g) 6Ni alloy. Isothermally transformed at 280 ℃ for 12 weeks.

Fig. 4.5: Optical micrographs of the 6Ni alloy.

4.2.2 Hardness Tests

Hardness data are shown in fig. 4.6. The hardness values of quenched fully martensitic samples are included for reference since the formation of bainite leads to a reduction in hardness, depending on the fraction of bainite. The trends in fig. 4.6 can easily be understood by the results of dilatometry and optical micrographs.

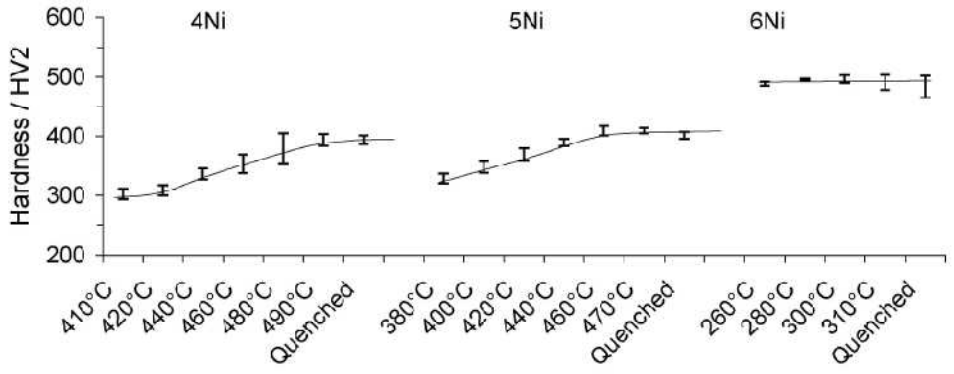

Fig. 4.6: Vickers hardness data measured using a 2 kg load. The temperatures correspond to isothermal transformation experiments.

4.2.3 X-ray Diffraction

X-ray diffraction (XRD) was conducted to examine whether austenite was retained. As seen in fig. 4.1, retained austenite transformed to martensite before sample reached room temperature. However it is necessary to check this once again with high accuracy. Retained austenite could not be detected, as shown fig. 4.7.

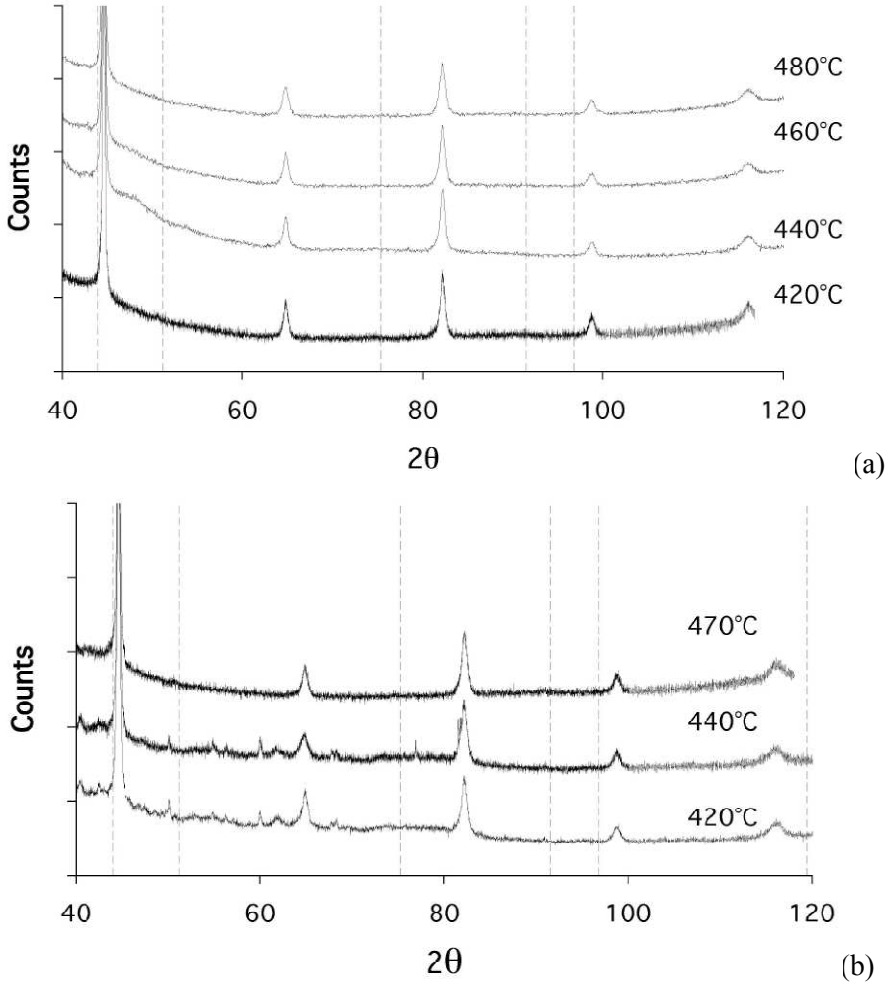

Fig. 4.7: X–ray diffraction patterns taken using CuK_{α} radiation. The ferrite peaks, in ascending order of 2θ can be indexed as 110, 002, 121, 022 and 031 respectively. The positions of possible austenite peaks are marked as lines, and in ascending order of 2θ are 111, 200, 220, 113, 222, and 004 respectively. Transformation temperatures are also indicated. (a) Sample 4Ni, (b) sample 5Ni.

4.2.4 Transmission Electron Microscopy

Transmission electron micrographs of the 4Ni and 5Ni alloys are shown in fig. 4.8, illustrating the typical thin-platelets separated by residual carbon-enriched austenite which decomposes in this alloy on cooling. Martensitic regions are therefore also seen in the figures.

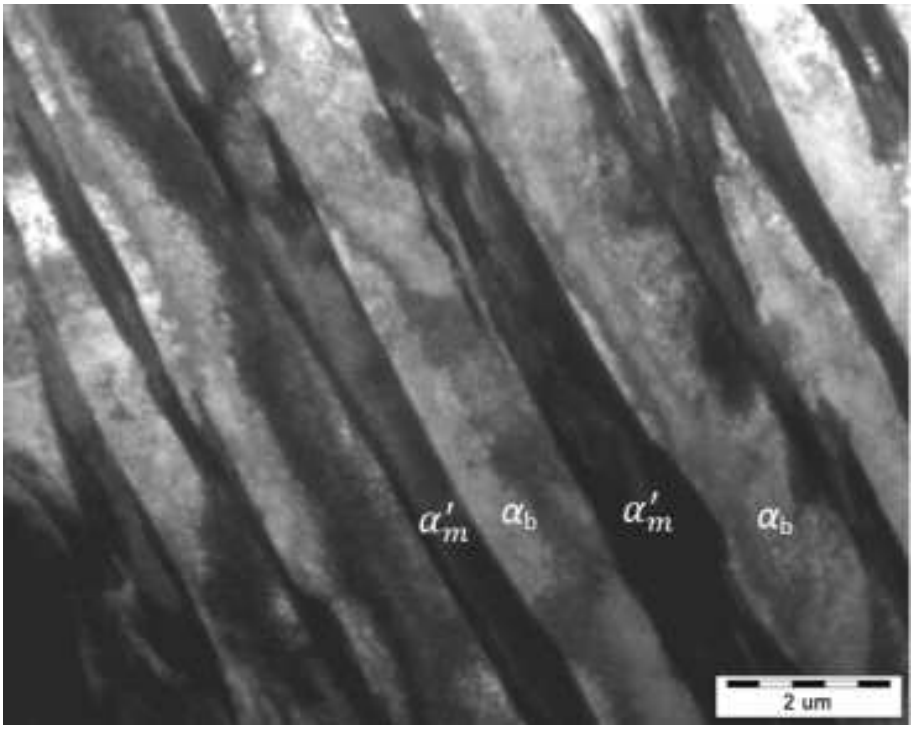

(a) 4Ni alloy. Isothermally transformed at 460 ℃, showing a mixture of bainitic ferrite platelets separated by regions of martensite.

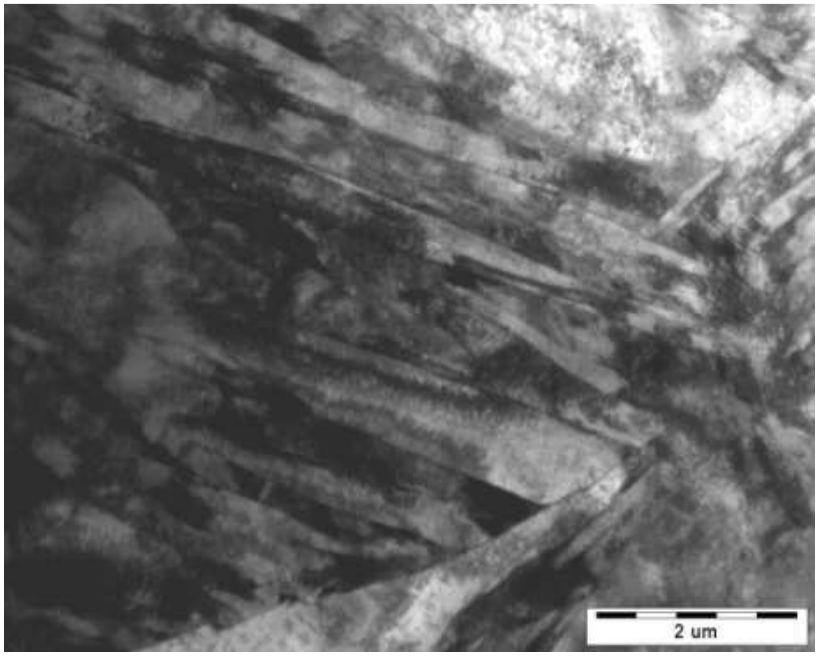

(b) 4Ni alloy. Isothermally transformed at 480 ℃, martensitic region.

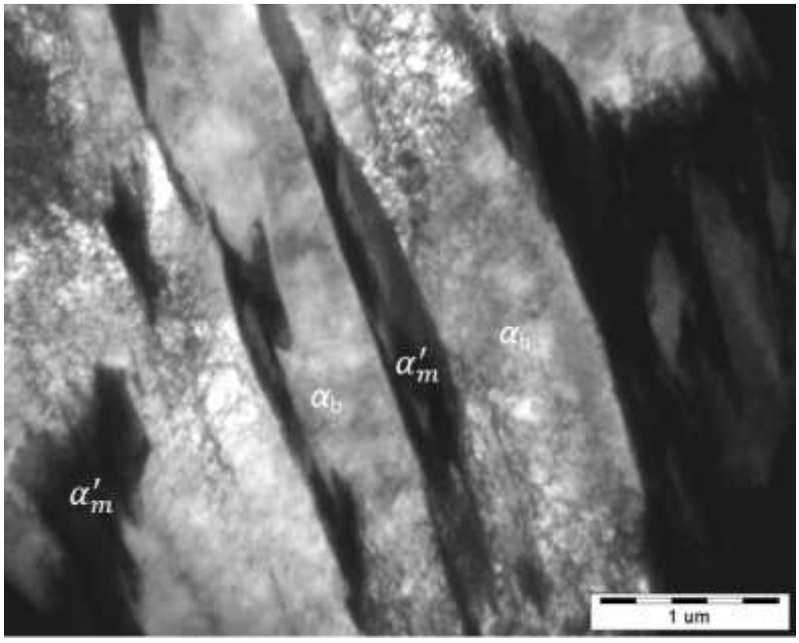

(c) 5Ni alloy. Isothermally transformed at 440 ℃, showing a mixture of bainitic ferrite platelets separated by regions of martensite.

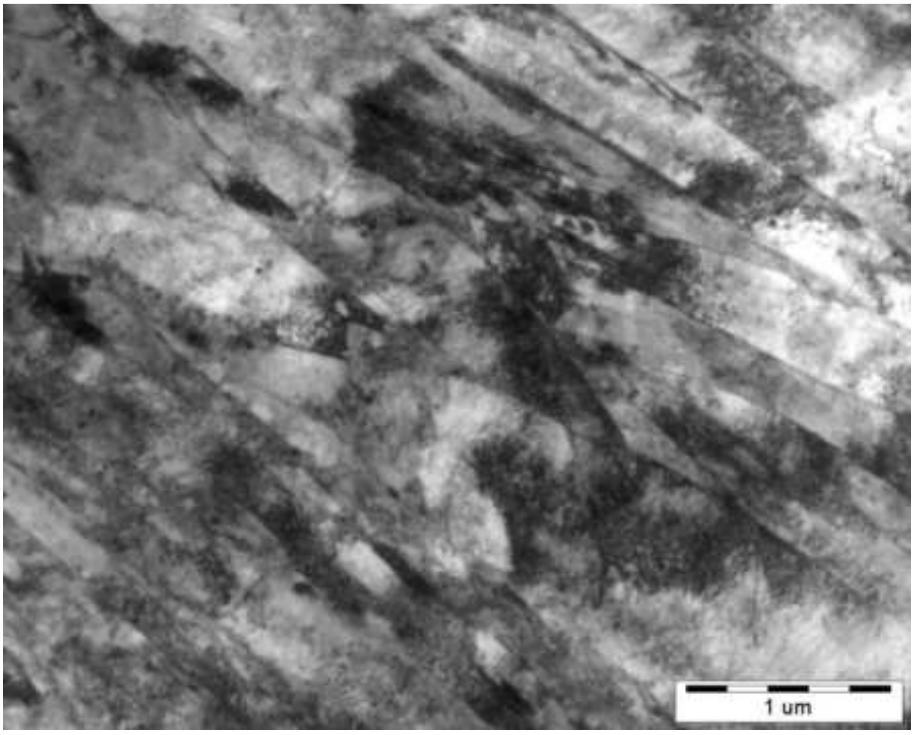

(d) 5Ni alloy. Isothermally transformed at 440 ℃, Martensitic region.

Fig. 4.8: TEM micrographs of 4Ni and 5Ni alloys.

Interesting features are revealed for the 6Ni alloy (fig. 4.9), which was transformed at quite a significant undercooling for long time. It is seen that there is a coalescence process at play in which fine platelets merge at their trailing edges to form coarser blocks. The elastically accommodated molar strain energy due to large strain, accompanied by displacive transformation, is given by (Christian, 1958)

$$G_S = \frac{\mu V_m}{1-\nu}\frac{\pi c}{4a}(\delta^2 + 0.5(2-\nu)s^2) \qquad (4.2)$$

where c is the plate thickness, a is the plate length, ν is the Poisson ratio, μ is the shear modulus of austenite, and V_m is the molar volume of the austenite. Coalescenced bainite has a large ratio of thickness to length, so its strain energy is large. Coalescence only occurs when the driving force available is large.

The fine platelets are of the order 20 nm thick but the coalesced regions (marked 'A' and 'B' in fig. 4.9b) are much coarser. This coalescence of bainite platelets has previously been reported in steels (Bhadeshia and Edmonds, 1979; Chang and Bhadeshia, 1996) and more recently in weld metals (Keehan *et al*., 2006a; 2006b; 2006c). Bhadeshia (2006b) reviewed the subject and the mechanism may be summarised as follows.

Coalesced bainite begins as a series of adjacent, identically oriented platelets of ferrite only marginally separated by films of austenite. As the platelets lengthen, they accelerate and coalesce. The carbon is then trapped in the ferrite, either to precipitate later or to partly partition into the residual austenite at the peripheries of the cluster of platelets. Such coalescence can only occur when the driving force available is sufficient to sustain the greater strain energy associated with the coarser plates.

Of relevance here is the relatively low carbon concentration and the reduced transformation temperature which permits the individual platelets to develop without intervening films of austenite, leading to the coalescence process. Although not proven here, the coalescence process works against the development of a fine microstructure and hence may be a limiting factor in the design of steels in which substitutional solutes are utilised to suppress the transformation temperature.

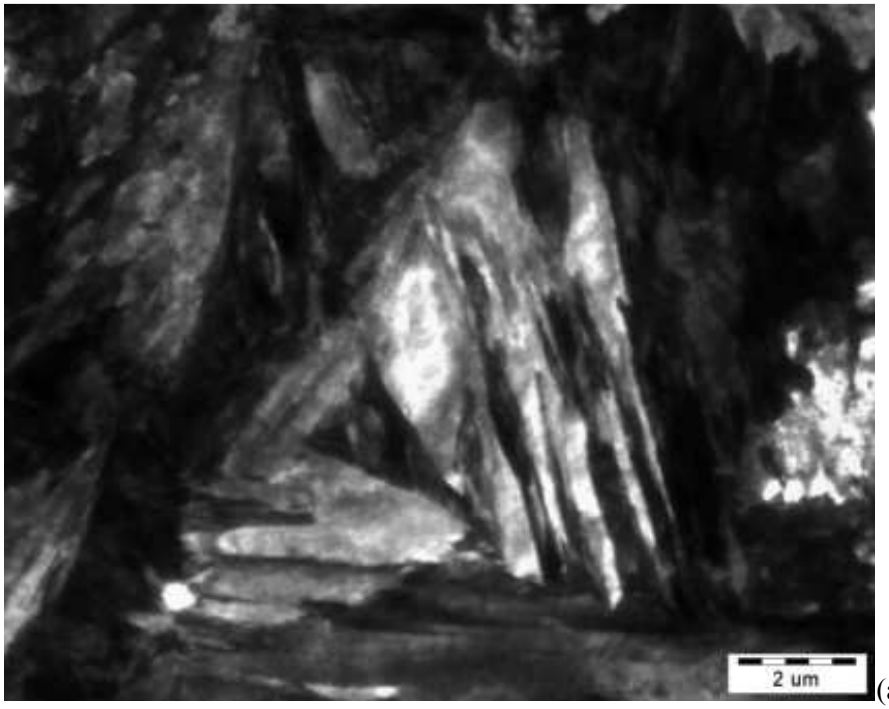

(a)

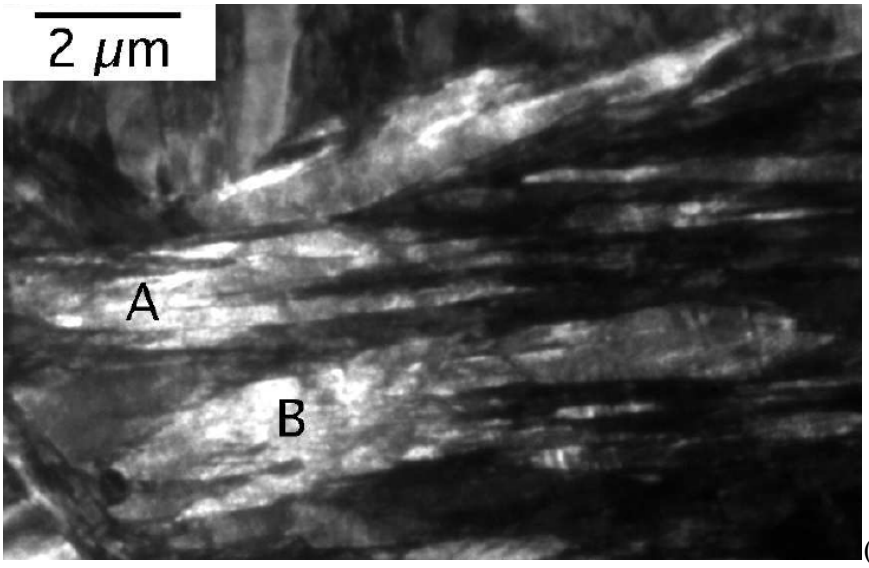

(b)

Fig. 4.9: 6Ni alloy, transformed isothermally at 280 ℃ for 12 weeks. (b) The annotations 'A' and 'B' mark regions where coalescence has occurred – the participating platelets are towards the right of each coalesced region.

4.3 Bainite-Start Temperatures

Based on dilatometric and characterization data, the 4Ni alloy at 490 ℃ failed to produce bainite so it can be concluded that 480 ℃ $< B_S <$ 490 ℃ since bainite was observed on transformation at 480 ℃. The B_S temperature of the 4Ni alloy is taken to be 485 ± 10 ℃, where the stated uncertainty is probably twice as large as the experiments might indicate, to allow for greater statistical confidence in the interpretation of the data. The B_S for 5Ni alloy was similarly established to be 465 ± 10 ℃.

There is a greater uncertainty for alloy 6Ni because of the very slow transformation rate but from the dilatometric data B_S is likely to be less than 300 ℃ and has been assumed to be 300 ± 15 ℃.

4.4 Analysis of the Transformation Temperatures

M_S and B_S temperatures measured in this work are shown in fig. 4.10 along with thermodynamic calculations. All calculations presented here exploit MTDATA (NPL, 2006) combined with the SGTE database to evaluate the free energies of the phases, using an algorithm (Okumura) based on the rationalisation of transformations in steels (Bhadeshia, 1981a)

Both bainite and martensite must form below the T_0' temperature and this is indeed found to be the case. Consistent with the predictions in fig. 1.11, the difference between the B_S and M_S temperatures decreases as the nickel concentration increases. It's only 30 ℃ for 6Ni alloy. It is interesting that this is one of the conditions for the onset of coalesced bainite (Andrén *et al*., 2006).

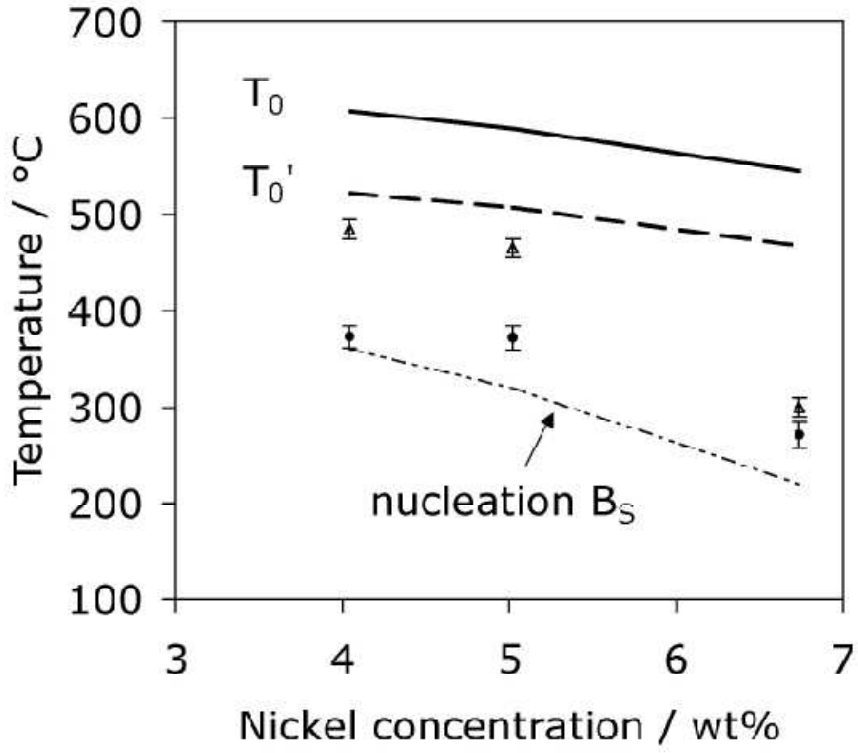

Fig. 4.10: Calculated T_0 and T_0' curves and measured martensite–start (circles) and bainite–start temperatures (triangles). The calculated nucleation–limited B_S is also illustrated.

Bainite-start temperatures based on dilatometric data were discussed in chapter 4.1 and are consistent with the fig. 4.10. B_S=T_0', which appears to the case for the 4Ni and 5Ni alloys as shown in fig. 4.10. However, the nucleation condition becomes controlling when the transformation is suppressed by alloying because of the reduced thermal activation. It is reasonable therefore for the measured B_S to be closer to the nucleation limited B_S for alloy 6Ni and well below T_0'. The measured B_S should not of course be above that calculated, as is the case for alloy 6Ni, but the reason for this is the exceptionally high transformation time used, which is not catered for by the original derivation of the universal nucleation function. The original work utilised a detectable nucleation rate at the highest transformation temperature (Bhadeshia, 1981a), fitted empirically to ordinary steels listed in an

atlas of isothermal transformation diagrams. Naturally, if a much lower detectable nucleation rate is defined by using an excessively large transformation time then the calculated B_S would increase to any point below the T_0' temperature. There clearly is a need to improve interpretation in order to deal with very slow transforming steels which have now assumed technological significance (Bhadeshia, 2004). In essence, for steels in which $B_S < T_0'$, it should be possible by using long heat treatments to eventually obtain bainite. If there is no limit placed on the heat–treatment time then the bainite–start temperature must be given by T_0' assuming that other transformations which normally are kinetically disadvantaged relative to bainite, do not intervene.

Finally, it is worth emphasising that with the 6Ni alloy which is nucleation limited, $B_S \ll T_0'$ which means that there is excess free energy available to sustain the greater strain energy associated with the coalescence process. This is not the case with the 4Ni and 5Ni alloys where coalescence is not observed.

4.5 Summary

Isothermal experiments and comprehensive metallographic experiments were conducted on the 4Ni, 5Ni and 6Ni alloys. The behaviour of the 4Ni and 5Ni alloys can be understood by the theory. The gap between M_S and B_S decreases as nickel alloying increases as predicted in fig. 1.11. Fig. 1.11 predicts that B_S would be below M_S, which means that bainite formation is impossible. However, bainite in the 6Ni alloy was observed. The reason is that the 6Ni used exceptionally long reaction time. The theory predicts that bainite reaction is impossible in the 6Ni alloy based on nucleation criterion. If infinite reaction time is allowed, every steel could satisfy the nucleation criterion. That is why bainite was formed in the 6Ni alloy. It's needed to improve the universal nucleation function concept in order to include very slow reaction steels.

It's possible to make bainite temperature as low as 280 ℃ using substitutional alloying and long reaction time. But low temperature, well below T_0', caused coalescence process which cancels the advantage of low temperature transformation.

Ⅴ. Summary and Future Work

5.1 Summary

The aim of this study was to examine the possibility of low-carbon super-bainite from a fundamental of view. During the study, uncertainties in dilatometric M_S were recognized. They were systemically analysed, and a method was proposed in which dilatometric data are interpreted by defining the first onset of transformation to be that at which a critical strain is achieved relative to the thermal contraction of the parent phase. The critical strain is calculated for 1 vol.% martensitic transformation assuming that the latter occurs at room temperature, by using equations for the lattice that the method is reproducible and emphasises that transformation start temperature should be quoted with the value of the critical strain used to interpret the dilatometric data.

In previous work, it has been shown that incredibly fine bainitic microstructures can be produced in bulk steel by suppressing the bainite transformation temperature, primarily by alloying with about 1 wt% carbon. The aim in the present work was to use substitutional solutes to achieve the same purpose while keeping the carbon concentration small.

It is found that the bainite-start temperature can indeed be suppressed in this way, but unlike the high-carbon steels, the difference between B_S and M_S decreases dramatically at high solute concentrations, as predicted theoretically. Furthermore, $B_S \ll T_0'$ so that there is excess free energy available during the course of transformation. Consequently, the fine platelets of bainite that are initiated tend to coalesce during the growth stage, perhaps negating the advantage of transforming at low temperatures. The work has also highlighted the need for improved interpretation of transformation–start temperatures in order to cope with very slow reaction at low homologous temperatures.

5.2 Future Work

Examinations of the 6Ni alloy revealed the possibility of low-carbon super-bainite even though coalescence process can cancel the advantage of low-temperature transformation. Its mechanical properties will be tested. Coalescence process and character of cementite precipitation will also be investigated.

The effects of carbon and nickel on transformation temperatures have been predicted theoretically in other works, and the effect of nickel was investigated in this work. A technique which is able to make alloys which that have a composition gradient would be helpful. Alloys which have a carbon or nickel gradient will be produced and investigated.

The ultimate purpose of this work was to achieve low-temperature, low-carbon super-bainite. A new alloy which can transform to bainite at low temperature, avoiding coalescence, will be designed based on knowledge of bainite transformation theory and this study.

VI. References

Ali, A. and Bhadeshia, H. K. D. H.: Aspects of the nucleation of Widmanstätten ferrite, *Materials Science and Technology*, Vol. 6 (1990) pp. 781-784

Andrén, H.-O., Keehan, E., Karlsson, L. and Svensson, L-E.: New developments with C-Mn-Ni high strength steel weld metals: Properties. Welding Journal, Reseach Supplement, Vol. 85 (2006) pp. 211s-218s

Bain, E. C.: The nature of martensite, *Trans. AIME*, Vol. 70 (1924) pp. 25-46

Bhadeshia, H. K. D. H.: A rationalisation of shear transformation in steels, *Acta Metallurgica*, Vol. 29 (1981a) pp. 1117-1130

Bhadeshia, H. K. D. H.: The driving force for martensitic transformation in steels, *Metal Science*, Vol. 15 (1981b) pp. 175-177

Bhadeshia, H. K. D. H.: Thermodynamic extrapolation and the martensite-start temperature of substitutionally alloyed steels, *Metal Science*, Vol. 15 (1981c) pp. 178-180

Bhadeshia, H. K. D. H: MAP_STEEL_MUCG46
http://www.msm.cam.ac.uk/map/steel/programs/mucg46-b.html (1987)

Bhadeshia, H. K. D. H.: New bainitic steels by design, *Modelling and simulation for materials design*, National Research Institute for Metals, Japan, (1998) pp. 227-232

Bhadeshia, H. K. D. H.: Neural networks in materials science, ISIJ International, Vol. 39 (1999) pp. 966-979

Bhadeshia, H. K. D. H.: *Bainite in Steels*. IOM Communications Ltd, London, second edition, (2001)

Bhadeshia, H. K. D. H.: Hard Bainite, *Solid→Solid Phase Transformation in Inorganic Materials*, Vol. 1 (2005a) pp. 469-484

Bhadeshia, H. K. D. H.: High performance bainitic steels, *Materials Science Forum*, 500-501 (2005b) pp. 63-74

Bhadeshia, H. K. D. H.: Large Chunks of Very Strong Steel, *Millenium Steel,* Vol. 5 (2004) pp. 25-28

Bhadeshia, H. K. D. H.: Bainitic Bulk-Nanocrystalline steel, *The 3rd international Conference on Advanced Structural Steels*, (2006a)

Bhadeshia, H. K. D. H.: Coalesced bainite. *Transactions of the Indian Institute of Metal*, Vol. 59 (2006b) pp. 689-694

Bhadeshia, H. K. D. H.: The nature, mechanism and properties of strong bainite, *Proceedings of the 1st International Symposium on Steel Science (IS3-2007)*, Iron and Steel Society of Japan (2007)

Bhadeshia, H. K. D. H. and Edmonds, D. V.: The bainite transformation in a silicon steel, *Metallurgical transactions A*, Vol. 10A (1979) pp. 895-907

Bhadeshia, H. K. D. H. and Waugh, A. R.: Bainite: An atom-probe study of the incomplete reaction phenomenon. *Acta Metallurgica.*, Vol. 30 (1982) pp. 775-784

Bhadeshia, H. K. D. H., David, S. A., Vitek, J. M. and Reed, R. W: Stree-induced transformation to bainite in a Fe-Cr-Mo-C pressure vessel steel, *Materials Science and Technology*, Vol. 7 (1991) pp. 686-698

Brofman, P. J. and Ansell, G. S.: On the effect of fine grain size on the M_S temperature in Fe-27 Ni-0.025 C alloys, Metallurgical Transactions A, Vol. 14A (1983) pp. 1929-1931

Caballero, F. G., Bhadeshia, H. K. D. H., Mawella, K. J. A., Jones, D. G. and Brown, P.: Very strong low temperature bainite. *Materials science and technology*, Vol. 18 (2002) pp. 279-284.

Caballero, F. G. and Bhadeshia, H. K. D. H.: Very strong bainite, *Current Opinion in Solid State and Materials Science*, Vol. 8 (2005) pp. 251-257

Caballero, F. G., Miller, M. K., Babu, S. S. and Garcia-Mateo, C.: Atomic scale observations of bainite transformation in a high carbon high silicon steel, *Acta Materialia*, Vol. 55 (2007) pp. 381-390

Capdevila, C., Caballero, F. G and de Andrés, C. G.: Determination of M_S temperature in steels: A Bayesian neural network model, *ISIJ International*, Vol. 42 (2002) pp.894-902

Capdevila, C., Caballero, F. G and de Andrés, C. G.: Analysis of effect of alloying elements on martensite start temperature of steels, Materials Science and Technology, Vol. 19 (2003) pp. 581-586

Chang, L. C: Bainite transformation in high-silicon steels. Metallurgical and Materials Transactions A, Vol. 30 (1999) pp. 909-916

Chang, L. C and Bhadeshia, H. K. D. H.: Microstructure of lower bainite formed at large undercoolings below the bainite start temperature. *Materials Science and Technology*, Vol. 12 (1996) pp. 233-236

Christian, J. W.: Accommodation strains in martensite formation, and the use of a dilatation parameter, *Acta Metallurgica*, Vol. 6 (1958) pp. 377-379

Chupatanakul, S. and Nash, P.: Dilatometric measurement of carbon enrichment in austenite during bainite transformation, *Journal of Materials Science*, Vol. 41 (2006) pp. 4965–4969

De Weijer, A. P., Vermeulen, W. G., Morris P. F. and van der Zwaag: Prediction of martensite start temperature using artificial neural networks, Ironmaking Steelmaking, Vol. 23 (1996) pp. 433-437

Dyson, D. J. and Holmes, B.: Effect of alloying additions on the lattice parameter of austenite, Journal of the Iron and Steel Institute, 208 (1970) pp. 469-474

Garcia-Mateo, C., Caballero, F. G. and Bhadeshia, H. K. D. H.: Low temperature bainite, *Journal de physique*, Vol. 112 (2003a) pp. 285-288

Garcia-Mateo, C., Caballero, F. G. and Bhadeshia, H. K. D. H.: Hard bainite, *ISIJ International*, Vol. 43 (2003b) pp. 1238-1243

Garcia-Mateo, C., Caballero, F. G. and Bhadeshia, H. K. D. H.: Development of hard bainite. *ISIJ International*, Vol. 43 (2003c) No. 8 pp. 1238-1243.

Garcia-Mateo, C. and Bhadeshia, H. K. D. H.: Nucleation theory for high-carbon bainite, *Materials Science and Engineering A*, Vol. 378A (2004) pp. 289-292

Ghosh, G. and Olson, G. B.: Kinetics of FCC→BCC heterogeneous martensitic nucleation. Part I: The critical driving force for athermal nucleation, *Acta Metallurgica et Materialia*, Vol. 42 (1994) pp. 3361-3370

Ghosh, G. and Olson, G. B.: Computational Thermodynamics and the Kinetics of Martensitic transformation, *J. Phase Equilb.*, Vol. 22 (2001) No. 3, pp. 199-207

Kaufman, L., Clougherty, E. V. and Weiss, R. J.: The lattice stability of metals-III. Iron, *Acta Metallurgica*, Vol. 11 (1963) pp. 323-335

Keehan, E., Karlsson, L. and Andrén, H.-O.: Influence of C, Mn and Ni on strong steel weld metals: Part 1, effect of nickel. *Science and Technology of Welding and Joining*, Vol. 11 (2006a) pp. 1-8

Keehan, E., Karlsson, L., Andrén, H.-O. and Bhadeshia, H. K. D. H.: Influence of C, Mn and Ni on strong steel weld metals: Part 2, increased impact toughness. *Science and Technology of Welding and Joining*, Vol. 11 (2006b) pp. 9-18

Keehan, E., Karlsson, L., Andrén, H.-O. and Bhadeshia, H. K. D. H.: Influence of C, Mn and Ni on strong steel weld metals: Part 3, increased strength. *Science and Technology of Welding and Joining*, Vol. 11 (2006c) pp. 19-24

Langford, G. and Cohen, M.: Calculation of cell-size strengthening of wire-drawn iron, *M Met. Trans.* Vol. 1 (1970) no. 5 pp. 1478-1480.

Lawson, R. D., Matlock, D. K. and Krauss G.: An etching technique for microalloyed dual-phase steels, *Metallography*, Vol. 13 (1980) pp. 71-87

LePERA, F. S.: Improved etching technique for the determination of percent martensite in high-strength dual-phase steels, *Metallography*, Vol. 12 (1979) pp. 263-268

Mackay, D. J. C.: Information theory, influence and learning algorithms, Cambridge, Cambridge University (2003)

Maki, T., Shimooka, S. and Tamura, I.: The temperature and morphology of martensite in Fe-31 pet Ni-0.23 pet C alloy, *Metallurgical Transactions*, Vol. 2 (1971) pp. 2944-2955

NPL: MTDATA. Software, National Physical Laboratory, Teddington, U. K., (2006)

Okumura, T.: MAP_STEEL_MTDATA, http;//www.msm.cam.ac.uk/map/steel/programs/MTTTDATA.html.

Olson, G. B., Cohen, M.: A general mechanism of martensitic nucleation: Part I. General concepts and the FCC-HCP transformation, *Metallurgical Transactions A*, Vol. 7A (1976) pp. 1897-1923

Olson, G. B., Tsuzaki, K., Cohen, M.: Statistical aspects of martensitic nucleation, *Material Research Symposium Proceedings*, Vol. 57 (1987) pp. 129-148

Peet, M., Babu, S. S., Miller, M. K. and Bhadeshia, H. K. D. H.: Three-dimensional atom probe analysis of carbon distribution in low-temperature bainite, *Scripta Materialia*, Vol. 50 (2004) pp. 1277-1281

Pereloma, E. V., Timokhina, I. B., Miller, M. K. and Hodgson, P. D.: Three-dimensional atom probe analysis of solute distribution in thermomechanically processed TRIP steels, *Acta Materialia*, unpublished (2007).

Singh, S.B. and Bhadeshia, H.K.D.H.: Estimation of bainite plate-thickness in low-alloy steels, *Materials Science and Engineering A,* Vol. 245 (1998) pp. 72–79

Swallow, E. and Bhadeshia, H. K. D. H.: High resolution observations of displacements caused by bainitic transformation, *Materials Science and Technology*, vol. 12 (1996) pp. 121-125.

Takahashi, M. and Bhadeshia, H. K. D. H.: A model for the transition from upper to lower bainite*, Materials Science and Technology*, Vol. 6 (1990) pp.592-603.

US National Bureau of Standards: X-ray powder data file (circ. 539 4 3), card for ferritic iron, (1955)

Wang, J. J., Van der Wolk, P. J. and Van der Zwaag, S.: Determination of martensite start temperature in engineering steels part I. Empirical relations describing the effect of steel chemistry, *Metals Trans JIM*, Vol. 41 (2000) pp. 761-768

Yang, Hong-Seok and Bhadeshia, H. K. D. H.: Uncertainties in dilatometric determination of martensite start temperature, *Materials Science and Technology*, Vol. 23 (2007) pp. 556-560

Zener, C.: Kinetics of the decomposition of austenite. *Trans. AIME*, Vol. 167 (1946) pp.550-595

CURRICULUM VITAE

Name: Yang, Hong-Seok

E-mail: puremind@potsech.ac.kr

Date of birth: 11th August, 1980

Place of birth: Jeju, South Korea

Education

M. S. 2008, POSTECH (Pohang, Korea), Graduate Institute of Ferrous Technology, Computational Metallurgy Group.

B. S. 2006 POSTECH (Pohang, Korea), Department of Chemical Engineering.

Publications

Hong-Seok Yang and H. K. D. H. Bhadeshia: Uncertainties in dilatometric determination of martensite start temperature. *Materials Science and Technology,* Vol.23 (2007) pp. 556-560

Hong-Seok Yang and H. K. D. H. Bhadeshia: Designing low-carbon, low-temperature bainite. *Materials Science and Technology, In press*